https://doi.org/10.5194/essd-2026-802
Preprint. Discussion started: 18 November 2026
© Author(s) 2026. CC BY 4.0 License.



Open Access Earth System Science Data Discussions

Extending the NASA Ozone Column Retrievals to NOAA-20 OMPS: A Consistent NOAA-20 OMPS Total Column Ozone Data Record for 2018–2026

Kanghyun Baek[1,2], Can Li[1], Natalya A. Kramarova[1], Gordon Labow[3], Glen Jaross[1], Bradford L. Fisher[3], Jerry R. Ziemke[1,4], Stacey M. Frith[1,5]

[1]Atmospheric Chemistry and Dynamics Laboratory, NASA Goddard Space Flight Center, Greenbelt, MD, USA
[2]Goddard Earth Sciences Technology and Research (GESTAR) / University of Maryland Baltimore Co, Maryland, USA
[3]Science & Technology Corporation (STC), Hampton, VA, USA
[4]Morgan State University, Baltimore, MD, USA
[5]ADNET Systems, Inc., Lanham, MD, USA

Correspondence to: Kanghyun Baek (kanghyun.baek@nasa.gov)

Abstract. Long-term satellite records of total column ozone are essential for monitoring stratospheric ozone recovery and maintaining continuity in global ozone climate data records. The Ozone Monitoring Instrument (OMI) aboard Aura and the Ozone Mapping and Profiler Suite (OMPS) Nadir Mapper aboard the Suomi National Polar-orbiting Partnership (SNPP) have provided key components of the NASA total ozone record. Here, we describe a NOAA-20 OMPS (N20/OMPS) total column ozone (TCO) dataset for 2018–present, generated with the NASA Total Ozone Mapping Spectrometer Version 8 (TOMS V8) retrieval algorithm. N20/OMPS nadir radiances were cross-calibrated against SNPP/OMPS, after which the off-nadir N20/OMPS pixels were calibrated relative to the corrected N20 nadir reference. The resulting N20/OMPS TCO record is intended to extend the SNPP/OMPS-based NASA ozone record into the Joint Polar Satellite System (JPSS) era. We evaluate the N20/OMPS retrievals through comparisons with SNPP/OMPS, an independent NOAA NESDIS N20 product, and Dobson observations from 44 stations worldwide. Seasonal and monthly gridded comparisons show strong agreement between N20/OMPS and SNPP/OMPS, with correlations near unity, monthly RMSE values of about 1.2 DU, and mean biases generally within a few tenths of a percent. The N20 minus SNPP differences show no pronounced dependence on solar zenith angle, total ozone amount, or latitude. From 2018 to 2025, the monthly mean N20 minus SNPP difference is 0.41 ± 0.49 DU. The fitted relative drift is −0.053 DU yr^{-1} (95 % confidence interval: −0.096 to −0.010 DU yr^{-1}), equivalent to approximately −0.18 % per decade; although statistically significant, its magnitude is small. NASA N20 retrievals are more consistent with NASA SNPP than the NOAA N20 V8TOz EDR for the cases examined, as expected because the present calibration was designed to maximize continuity between the NASA SNPP and N20 records. Comparisons with Dobson observations yield a correlation coefficient of 0.96, an RMSE of 2.34 DU, and a mean relative bias of 0.18 ± 3.84 %, comparable to the corresponding SNPP/OMPS performance. These results demonstrate that the new N20/OMPS dataset provides a consistent extension of the SNPP/OMPS-based NASA total ozone record. The dataset is available from NASA Earthdata at https://doi.org/10.5067/T4BRYY6L5HFD (Baek and Li, 2026).

https://doi.org/10.5194/essd-2026-802
Preprint. Discussion started: 18 November 2026
© Author(s) 2026. CC BY 4.0 License.



Open Access Earth System Science Data Discussions

1 Introduction

Stratospheric ozone absorbs harmful solar ultraviolet (UV) radiation, whereas tropospheric ozone is a toxic air pollutant that adversely affects human health and damages vegetation and ecosystems (Crutzen, 1979; Jacob et al., 1999). The Montreal Protocol and its amendments established international controls on ozone-depleting substances. Sustained global observations are essential for assessing the resulting recovery of the ozone layer and its interactions with climate change (Fang et al., 2019; WMO, 2014).

Satellite remote sensing has been a cornerstone of global ozone monitoring because it provides global, long-term observations that cannot be achieved by ground-based networks alone. NASA has measured ozone from space since the launch of the Backscatter Ultraviolet (BUV) instrument aboard Nimbus-4 in 1970. This was followed by a series of UV backscatter instruments, including the Solar Backscatter Ultraviolet (SBUV) instruments, the Total Ozone Mapping Spectrometer (TOMS) aboard Nimbus-7, Meteor-3, Earth Probe and ADEOS (McPeters et al., 2000), and the SBUV/2 instruments aboard NOAA polar-orbiting satellites (McPeters et al., 2013). The launch of TOMS in 1978 marked the first mission dedicated to producing global maps of total column ozone from space (McPeters et al., 1996). Subsequent instruments, including the Global Ozone Monitoring Experiment (GOME; Burrows et al., 1999), the SCanning Imaging Absorption spectroMeter for Atmospheric CHartographY (SCIAMACHY; Bovensmann et al., 1999), the Ozone Monitoring Instrument (OMI; Levelt et al., 2006), the Ozone Mapping and Profiler Suite Nadir Mapper (OMPS-NM; Flynn et al., 2014), and the TROPOspheric Monitoring Instrument (TROPOMI; Veefkind et al., 2012), have built upon this heritage and have enabled multi-decadal monitoring of global ozone distributions.

Long-term ozone records have been developed from several complementary satellite measurement approaches. Nadir-profiler measurements, including BUV, SBUV, and SBUV/2, have been used to construct internally consistent merged ozone records for long-term ozone trend studies, such as the Merged Ozone Data (MOD) time series (McPeters et al., 2013; Frith et al., 2014). In parallel, nadir-mapping instruments such as TOMS, OMI, and OMPS-NM provide global TCO maps with high spatial coverage, which are widely used to monitor the horizontal distribution of ozone and its temporal variability (McPeters et al., 1996; Levelt et al., 2006; Flynn et al., 2014). Although these profiler-based and mapper-based records are complementary, they differ in measurement geometry and retrieval characteristics and therefore require separate calibration and consistency assessments.

For the mapper-based TCO record, the OMPS-NM instrument aboard the Suomi National Polar-orbiting Partnership (SNPP) spacecraft, launched in 2011, has served as the primary successor to earlier NASA TOMS and OMI observations. The SNPP/OMPS TCO product is processed with the NASA Version 8 total ozone algorithm and has been improved through calibration updates that support stable long-term measurements (Seftor et al., 2014; Kramarova et al., 2014; McPeters et al., 2019). Extending this record to a new satellite platform requires careful treatment of sensor-specific calibration, cross-track dependence, wavelength-dependent reflectivity effects, and retrieval sensitivities.

https://doi.org/10.5194/essd-2026-802
Preprint. Discussion started: 18 November 2026
© Author(s) 2026. CC BY 4.0 License.

Open Access Earth System Science Data Discussions

Previous work by NOAA addressed related calibration and consistency issues for OMPS total ozone retrievals. Zhang et al. (2023) tracked calibration changes in the Version 8 total ozone algorithm by applying broadband-channel adjustments and soft calibration to SNPP/OMPS and N20/OMPS retrievals. Their study showed that soft calibration improved the stability and consistency of total column ozone and aerosol index products between the two platforms and reduced cross-track inconsistencies, although residual solar- and viewing-zenith-angle-dependent biases remained.

An updated N20/OMPS Level-1B (L1B) radiance record produced by the NASA Goddard Space Flight Center team became available in 2026, providing the basis for a renewed assessment of N20 total ozone retrievals. As SNPP/OMPS approaches the later stage of its mission, retrievals based on the updated N20/OMPS L1B record must be evaluated for their ability to provide a consistent extension of the SNPP/OMPS-based NASA mapper TCO record. N20/OMPS has finer native spatial sampling than SNPP/OMPS; this difference is treated explicitly in the cross-calibration and comparison procedures rather than serving as the primary motivation for the calibration.

The goal of this study is to develop and evaluate a consistent N20/OMPS TCO dataset that extends the NASA ozone data record beyond SNPP and provides continuity for future JPSS OMPS missions.

The rest of the paper is organized as follows. Section 2 describes the N20/OMPS data, the NASA total ozone retrieval algorithm, and the soft-calibration approach used in this study. Section 3 presents the evaluation of the N20/OMPS TCO dataset, and Sect. 4 summarizes the conclusions. Data availability and supporting material are provided after Appendix A.

2 Data and methodology

2.1 N20/OMPS Nadir Mapper

NOAA-20 is the follow-up mission to Suomi NPP and was launched in November 2017 into an afternoon Sun-synchronous orbit with an equator-crossing time near 13:30 local time. During the early part of the mission, NOAA-20 flew in nearly the same orbital plane as SNPP, observing the same region about 50 min earlier. After NOAA-21 entered the constellation, the relative orbital phasing was adjusted, and NOAA-20 now precedes SNPP by about 25 min. The overlapping afternoon-orbit observations from SNPP, NOAA-20, and NOAA-21 provide the observational basis for maintaining continuity in OMPS ozone measurements.

The NOAA-20 OMPS payload includes two nadir-viewing sensors, NM and NP, whereas the SNPP OMPS payload also includes the Limb Profiler. The NM measurements used here consist of ultraviolet radiances scattered from the Earth–atmosphere system and solar irradiances over approximately 300–380 nm. The spectral sampling is about 0.42 nm, with a spectral resolution of approximately 1.0 nm full width at half maximum. The 110° cross-track viewing range corresponds to a ground swath of roughly 2800 km, providing nearly daily global coverage (Flynn et al., 2014; Seftor et al., 2014; Xiong et al., 2019).

The NM detector is a configurable two-dimensional CCD array, with 340 pixels in the spectral dimension and 720 pixels in the spatial dimension (Seftor et al., 2014; Xiong et al., 2019). In the standard SNPP/OMPS-NM configuration, the spatial

https://doi.org/10.5194/essd-2026-802
Preprint. Discussion started: 18 November 2026
© Author(s) 2026. CC BY 4.0 License.



pixels are aggregated into 36 cross-track fields of view, producing an approximate nadir footprint of 50 km × 50 km with a 7.6 s integration and reporting period. N20/OMPS-NM uses a shorter 2.5 s integration time and finer spatial aggregation. At the beginning of the N20 mission, the spatial pixels were aggregated into 104 macro-pixels, giving an approximate nadir footprint of 17 km along track by 17 km across track. Beginning with orbit 6419 on 13 February 2019, the aggregation scheme was changed to 140 macro-pixels, reducing the nadir across-track footprint to approximately 13 km.

The different spatial sampling of N20/OMPS-NM and SNPP/OMPS-NM is explicitly accounted for in the cross-calibration. Selected N20 near-nadir pixels are aggregated to approximate the SNPP nadir footprint when the nadir adjustments are derived, whereas the native N20 sampling is retained in the final product.

2.1.1 Product format, structure, and key variables

The OMPS-N20 NMTO3-L2 Version 2.0 product is distributed as orbit-level HDF5 swath files. Each file contains measurements from the daylit portion of one orbit and typically includes 1201 along-track observations. The cross-track dimension contains 104 pixels before orbit 6419 on 13 February 2019 and 140 pixels thereafter. Additional dimensions comprise 12 wavelengths, four field-of-view corners, and 11 pressure levels. Variables are organized into four functional groups: AncillaryData, CalibrationData, GeolocationData, and ScienceData. Table 1 summarizes the variables most relevant to general users; complete definitions, metadata attributes, and bit assignments are provided in the product README (NASA GES DISC, 2026).

The primary science variable is ScienceData/ColumnAmountO3, which reports final TCO in DU. Pixel locations and boundaries are provided by the center and corner coordinates in GeolocationData, together with observation geometry and time. AlgorithmFlags identifies the retrieval branch; values 1 and 11 correspond to standard retrievals for non-snow/ice and snow/ice scenes, respectively. QualityFlags is a bit-packed variable. In this study, qflag denotes the integer value represented jointly by bits 0–3 of QualityFlags (equivalently, qflag = QualityFlags bitwise AND 15). For high-quality TCO, the recommended screening is AlgorithmFlags = 1 or 11 and qflag ≤ 1, retaining good samples and glint-contaminated samples for which the glint correction was applied. The product also includes Reflectivity331, cloud quantities, N-values and their soft-calibration adjustments, and UVAerosolIndex. The UVAerosolIndex field is included for retrieval diagnostics and aerosol correction and is not intended as a stand-alone science aerosol product.

Table 1. Summary of the principal variables in the OMPS-N20 NMTO3-L2 Version 2.0 product. Unless otherwise stated, pixel-level variables have dimensions DimAlongTrack × DimCrossTrack. The qflag used for screening is the integer value represented jointly by bits 0–3 of QualityFlags (equivalently, qflag = QualityFlags bitwise AND 15). Complete variable definitions, dimensions, metadata attributes, and bit assignments are provided in the product README (NASA GES DISC, 2026).

Group	*Variable*	*Description*	*Units/notes*
AncillaryData	CloudPressure; TerrainPressure	Optical centroid cloud pressure and terrain pressure	hPa

https://doi.org/10.5194/essd-2026-802
Preprint. Discussion started: 18 November 2026
© Author(s) 2026. CC BY 4.0 License.



CalibrationData	Wavelength	Wavelength grid used by the retrieval (DimWavelength = 12)	nm
GeolocationData	Latitude; Longitude	Pixel-center latitude and longitude	degrees north/east
GeolocationData	LatitudeCorner; LongitudeCorner	Coordinates of the four field-of-view corners	degrees north/east
GeolocationData	SolarZenithAngle; ViewingZenithAngle; RelativeAzimuthAngle	Sun–sensor geometry for each ground pixel	degrees
GeolocationData	UTC_CCDSDS_A; Time	UTC date-time string and TAI93 time for each along-track scan	string; s
ScienceData	ColumnAmountO3	Final total column ozone	DU
ScienceData	AlgorithmFlags	Retrieval branch: 0 skipped, 1 standard, 2 profile-shape adjusted, and 3 C-pair; add 10 for snow/ice	unitless
ScienceData	QualityFlags	Bit-packed output quality flag. qflag is obtained by interpreting bits 0–3 together; qflag = 0 is a good sample and qflag = 1 is glint contamination corrected	unitless
ScienceData	Reflectivity331	Effective scene reflectivity at 331 nm	unitless
ScienceData	fc; RadiativeCloudFraction	MLER cloud fraction and radiative cloud fraction	unitless
ScienceData	NValue; NValueAdjustment	Normalized radiance expressed as N-value and applied wavelength- and cross-track-row-dependent soft-calibration adjustment	unitless
ScienceData	UVAerosolIndex	UV aerosol index included for retrieval diagnostics and aerosol correction; not recommended as a stand-alone science aerosol product	unitless

2.2 The Total Ozone Mapping Spectrometer (TOMS) algorithm

The N20/OMPS TCO retrievals used in this study are produced with the NASA total ozone algorithm, which follows the heritage Total Ozone Mapping Spectrometer (TOMS) Version 8 algorithm framework. Detailed descriptions of the algorithm are provided in the OMI Algorithm Theoretical Basis Document (Bhartia and Wellemeyer, 2002) and in the SNPP OMPS Level-2 (L2) total ozone product documentation (NASA GES DISC, 2017). In this section, we provide a brief overview of the retrieval algorithm (Sect. 2.2.1) and then describe the updated soft-calibration procedure applied to N20/OMPS (Sect. 2.2.2).

2.2.1 Algorithm overview

Under most observing conditions, the NASA total ozone algorithm uses a weakly ozone-absorbing wavelength near 331.2 nm to characterize effective scene reflectivity and a strongly ozone-absorbing wavelength near 317.5 nm to retrieve total column ozone. The Brion–Daumont–Malicet ozone absorption cross sections are used in the retrieval (Daumont et al., 1992; Brion et al., 1993; Malicet et al., 1995). For larger ozone optical paths, typically at high solar or viewing zenith angles, the algorithm switches to a longer wavelength pair, using the channel near 360 nm to derive reflectivity and the 331.2 nm channel to retrieve ozone.

https://doi.org/10.5194/essd-2026-802
Preprint. Discussion started: 18 November 2026
© Author(s) 2026. CC BY 4.0 License.



Measured radiance-to-irradiance ratios are expressed as N-values, defined as $N = -100 \log_{10}(I/F)$, where I is the Earth radiance and F is the solar irradiance. This logarithmic formulation converts small multiplicative calibration errors in I/F into approximately additive offsets in N-value space. Cloud effects are treated using an optical centroid cloud pressure (OCCP) climatology derived from OMI OMCLDRR retrievals (Vasilkov et al., 2008) to estimate the ozone column below the effective cloud level. Further details of the heritage retrieval are provided by Bhartia and Wellemeyer (2002) and the SNPP OMPS L2 total ozone product documentation.

2.2.2 Soft-calibration approach

In this study, soft calibration refers to small empirical adjustments to measured N-values that reduce residual radiometric calibration errors. Retrieved TCO, scene reflectivity, and UVAI are used only as diagnostics or constraints for deriving the adjustments; they are not corrected a posteriori. The adjustments depend on wavelength and cross-track row but not on latitude, season, or time. They are intended to improve consistency between N20/OMPS and the established SNPP/OMPS TCO record without replacing the underlying L1B radiometric calibration or altering product trends. Appendix A provides the detailed scene-selection criteria, reference definitions, wavelength-specific equations, sign convention, and iteration procedure.

The soft-calibration adjustments were derived separately for the early-mission 104-row configuration and the later 140-row configuration because the cross-track sampling and spatial aggregation changed after orbit 6419 on 13 February 2019. The analysis used low-aerosol, mostly clear tropical dark-land scenes selected using constraints on latitude, solar zenith angle, surface type, surface reflectivity, ultraviolet color index, terrain, and snow or ice. These criteria limit geophysical variability and allow wavelength- and row-dependent calibration biases to be isolated.

The calibration procedure consists of two stages. In the first stage, N20/OMPS nadir N-value adjustments are derived using SNPP/OMPS nadir quantities as external references. Because N20/OMPS and SNPP/OMPS have different spatial resolutions, selected N20 near-nadir pixels are first aggregated to approximate the SNPP nadir footprint. The adjustment to 331 nm reflectivity channel is derived from differences over dark-scenes, using the lowest 10 % of R331 values within the screened dark-land sample ($0 < R331 < 0.15$). This wavelength is only weakly affected by ozone absorption and is therefore used primarily to constrain scene reflectivity. Adjustments at the ozone-sensitive wavelengths, 312, 317, and 322 nm, are derived by comparing N20 nadir radiances at each wavelength with the corresponding SNPP nadir reference. The 360 nm adjustment is derived independently and does not use SNPP as a reference. Instead, a Gaussian function is fitted to the N20 UVAI probability distribution over the screened dark-land scenes, and the 360 nm N-value adjustment is selected so that the fitted N20 UVAI mean approaches zero.

In the second stage, after the N20 nadir reference has been established, row-dependent N-value adjustments are derived for the remaining N20/OMPS off-nadir cross-track positions using the corrected N20 nadir retrievals as the internal reference. This step is designed to remove artificial cross-track biases across the swath. The row-dependent adjustments are derived separately for the reflectivity wavelength, the ozone-sensitive wavelengths, and the UVAI-related wavelength, so that residual

https://doi.org/10.5194/essd-2026-802
Preprint. Discussion started: 18 November 2026
© Author(s) 2026. CC BY 4.0 License.


cross-track biases in scene reflectivity, TCO, and UVAI are reduced consistently. Same as previously, the corrections are applied in N-value space to measured radiances.

The adjustments are derived iteratively, beginning with the reflectivity channel. The procedure generally converges within five to six iterations, after which the final wavelength- and row-dependent adjustment tables are applied to the measured N-values in the N20/OMPS TCO processing.

2.3 Reference and validation datasets

2.3.1 NASA SNPP/OMPS reference product

SNPP/OMPS total column ozone retrievals produced with the NASA total ozone algorithm were used as the primary satellite reference for evaluating the updated N20/OMPS TCO dataset. The purpose of the N20/OMPS product developed in this study is to continue the SNPP/OMPS-based NASA mapper TCO record into the JPSS era. SNPP/OMPS therefore provides the most direct satellite reference because it has the same nadir-mapping measurement concept and is processed within the NASA TOMS-Version 8 heritage retrieval framework.

The use of SNPP/OMPS as a reference also provides an important test of the soft-calibration strategy. As described in Sect. 2.2.2, the N20/OMPS soft-calibration adjustments were derived by matching N20/OMPS and SNPP/OMPS nadir retrievals for selected calibration periods and then deriving row-dependent adjustments relative to the corrected N20 nadir reference. It is therefore necessary to evaluate whether the resulting N20/OMPS retrievals remain consistent with SNPP/OMPS over the full overlapping period, across the full swath, and under a broad range of geophysical conditions, rather than only within the nadir calibration samples

The NASA SNPP/OMPS L2 total ozone product used in this study (OMPS_NPP_NMTO3_L2) is available via NASA's EarthData archive. SNPP/OMPS retrievals from March 2018 to December 2025 were used as the reference dataset for satellite-to-satellite comparisons and for preliminary screening of ground-based validation stations.

Unless otherwise stated, satellite-to-satellite comparisons were restricted to high-quality TCO retrievals. Specifically, we used retrievals over non-snow/ice scenes, corresponding to algorithm flag equal 1.

For the gridded comparisons, SNPP/OMPS and N20/OMPS L2 retrievals were mapped to daily 1° longitude × 1° latitude grids. Although both instruments fly in afternoon Sun-synchronous orbits, the local observation times are not identical; during much of the comparison period, N20/OMPS observed the same region approximately 25 min apart from SNPP/OMPS. To reduce sampling differences near the daily boundary, where the first and last swaths of a day may not have corresponding observations from both sensors, the first and last orbits in each daily swath set were excluded before constructing the daily grids. This procedure reduces artificial daily mean differences caused by incomplete temporal overlap rather than by retrieval or calibration differences.

https://doi.org/10.5194/essd-2026-802
Preprint. Discussion started: 18 November 2026
© Author(s) 2026. CC BY 4.0 License.



2.3.2 NOAA V8TOz total ozone product

The NASA N20/OMPS retrievals developed in this study were also compared with the NOAA OMPS Version 8 Total Ozone Environmental Data Record (V8TOz EDR) to characterize product-level differences between the NASA and NOAA processing approaches. The NOAA V8TOz EDR is part of the NOAA/NESDIS JPSS ozone processing system and is distributed through the NOAA Comprehensive Large Array-data Stewardship System (CLASS) under the JPSS_OZONE data family (NOAA CLASS, 2026). The NOAA-processed N20 V8TOz subset used in this study was obtained from NOAA CLASS for two comparison periods: 12 September 2020, which was one of the validation dates used by Zhang et al. (2023), and the full month of June 2020.

In the product comparisons, the NASA products are referred to as NASA N20 and NASA SNPP, whereas the NOAA-processed products are referred to as NOAA N20 and NOAA SNPP. This notation is used to avoid ambiguity when comparing TCO products generated from the same satellite platforms but produced with different processing systems. Both NASA and NOAA retrievals are based on the same TOMS Version 8 (V8) algorithm framework; however, the implementations differ in several aspects, including input L1B data, calibration tables, soft-calibration implementation, retrieval settings, row configuration, native spatial resolution, and processing environments. Therefore, the comparison with NOAA N20 is interpreted as a product-level comparison rather than as an isolated test of any single algorithm or calibration component.

Spatial resolution differences were also considered in the comparison. The NASA N20/OMPS dataset preserves the native high spatial resolution of N20/OMPS-NM, approximately $13 \times 17\ km^2$ at nadir for the 2020 comparison periods, whereas the NOAA V8TOz EDR is provided at an approximately $50 \times 50\ km^2$ nadir footprint and uses a different cross-track configuration. The NOAA V8TOz EDR is processed using 35 cross-track positions, whereas the NASA OMPS processing uses a different row configuration. Because of these differences, the quantitative comparison between NASA N20 and NOAA N20 was not performed by direct swath-level pixel matching. Instead, both products were screened using the same standard retrieval criterion, algorithm flag 1, the first and last orbits of each daily swath set were excluded to reduce UTC-day boundary sampling differences, and the remaining retrievals were mapped to daily 1° longitude × 1° latitude grids.

2.3.3 Ground-based Dobson observations

Ground-based Dobson spectrophotometer observations were used as the primary independent validation dataset for the updated N20/OMPS total ozone retrievals. Dobson measurements provide long-term daily total column ozone observations and have been widely used for validation of satellite ozone products. In this study, daily mean Dobson total ozone observations were obtained from the World Ozone and Ultraviolet Radiation Data Centre (WOUDC) for the period from March 2018 to December 2025. Because the Dobson data are provided as daily mean total ozone values, no additional temporal co-location was applied. For spatial matching, the nearest OMPS pixel within 50 km of each Dobson site was selected. A total of 73 Dobson sites were initially considered. Dobson stations were screened using SNPP/OMPS as the satellite reference before they were applied to the N20/OMPS validation. This screening was performed to ensure that the ground-based reference dataset

https://doi.org/10.5194/essd-2026-802
Preprint. Discussion started: 18 November 2026
© Author(s) 2026. CC BY 4.0 License.



was stable and internally consistent before being used to evaluate the new N20/OMPS product. Satellite observations have previously been used to assess the performance of ground-based ozone measurement networks and to identify potential problems in individual station records (Bojkov et al., 1988; Fioletov et al., 1999, 2008). This approach is justified because a given satellite product is processed consistently with a single retrieval algorithm, and satellite instrument characteristics generally change gradually; therefore, abrupt or anomalous changes in satellite–ground differences at individual sites are more likely to reflect issues in the ground-based record than changes in the satellite product.

Stations with fewer than 50 SNPP/OMPS–Dobson matchups were excluded. Additional screening used the correlation coefficient, regression slope, mean bias, and RMSE of the SNPP/OMPS–Dobson comparisons to identify outlying station records. After screening, 44 Dobson stations were retained for the independent validation of the updated N20/OMPS dataset; station information and validation statistics are provided in Table 2.

Table 2. Dobson stations retained for the independent comparison with the N20/OMPS TCO dataset and station-level comparison statistics. The table lists the 44 retained Dobson stations and provides, for each station, the number of satellite–Dobson matchups, RMSE, mean bias, correlation coefficient, regression slope, relative bias, and drift in percent per year. Bias and drift are calculated from N20/OMPS minus Dobson differences.

IDS	SITE	COUNTRY	LATITUDE	LONGITUDE	N	RMSE [DU]	MBE [%]	CORRELATION	SLOPE	TREND [%/YR]
268	Arrival Heights/McMurdo	Antarctica	-77.8	166.7	240	2.04	-0.49	0.9	0.9	0.250
101	Syowa	Japan	-69	39.6	383	2.18	0.77	0.91	0.93	0.113
233	Marambio	Antarctica	-64.2	-56.6	739	2.61	1.45	0.95	0.96	0.051
339	Ushuaia	Argentina	-54.8	-68.3	2462	2.36	1.16	0.95	0.98	-0.133
29	Macquarie Island	Australia	-54.5	159	2301	2.39	1.45	0.97	1.04	0.016
342	Comodoro	Argentina	-45.8	-67.5	2398	2.45	2.94	0.92	0.91	0.021
256	Invercargill	New_Zealand	-45	169.7	1509	2.07	-0.03	0.98	1.01	0.005
256	Lauder	New_Zealand	-45	169.7	1509	2.07	-0.03	0.98	1.01	-0.003
394	Broadmeadows	Australia	-37.7	144.9	309	1.79	0.26	0.98	1.03	-0.001
253	Melbourne Airport	Australia	-37.7	144.9	2639	2.13	-0.03	0.96	1.07	-0.016
91	Buenos Aires	Argentina	-34.6	-58.5	2453	2.25	-0.48	0.89	0.87	-0.024
340	Springbok	South_Africa	-29.7	17.9	2314	2.39	-1.34	0.81	0.72	-0.178
27	Brisbane	Australia	-27.4	153.1	2806	1.77	-1.13	0.94	0.95	-0.166
84	Darwin	Australia	-12.4	130.9	2758	1.8	-0.25	0.83	0.73	-0.161
2	Tamanrasset	Algeria	22.8	5.5	2690	1.83	0.4	0.91	0.84	-0.114
245	Aswan	Egypt	24	32.8	1299	2.25	-1.24	0.87	0.83	-0.097
190	Naha	Japan	26.2	127.7	22	1.82	1.53	0.92	1.02	0.028
10	New Delhi	India	28.5	77.2	2330	2.29	-0.99	0.86	0.75	0.024
152	Cairo	Pakistan	30.1	31.3	1339	2.12	-1.5	0.91	0.96	0.036
464	University of Tehran	Iran	35.7	51.4	1131	1.65	1.15	0.98	1.04	0.041

https://doi.org/10.5194/essd-2026-802
Preprint. Discussion started: 18 November 2026
© Author(s) 2026. CC BY 4.0 License.



14	Tateno/Tsukuba	Japan	36.1	140.1	1798	2.36	0.13	0.96	0.99	0.036
341	Fresno + Hanford	United_States	36.3	-119.6	1506	2.08	1.24	0.96	0.96	0.034
341	Hanford	United_States	36.3	-119.6	1506	2.08	1.24	0.96	0.96	0.032
213	El Arenosillo	Spain	37.1	-6.7	478	2.11	0.05	0.96	0.96	0.022
252	Seoul	Korea_Republic	37.6	126.9	1656	2.8	-0.21	0.91	0.91	0.019
107	Wallops Island	United_States	37.9	-75.5	966	1.73	0.05	0.98	1	0.016
293	Athens	Greece	38	23.7	438	1.91	0.26	0.97	0.97	0.013
82	Lisbon	Portugal	38.8	-9.1	853	1.84	0.51	0.97	0.99	0.007
208	Xianghe	China	39.9	116.7	2174	2.46	0.37	0.96	1.03	0.010
67	Boulder	United_States	40.1	-105.3	2689	2.18	-0.84	0.96	1	0.004
410	Amberd	Armenia	40.4	44.2	1680	2.62	2.01	0.9	0.9	-0.001
40	Haute Provence	France	43.9	5.7	2030	2.51	0.24	0.94	0.92	-0.014
226	Bucharest	Romania	44.5	26.1	1368	2.05	-0.17	0.97	1.01	-0.018
19	Bismarck	United_States	46.8	-100.8	712	2.48	-0.39	0.96	0.95	-0.014
20	Caribou	United_States	46.9	-68	150	2.84	-1.79	0.92	0.88	-0.018
99	Hohenpeissenberg	Germany	47.8	11	1494	1.93	0.61	0.98	1.02	-0.021
96	Hradec Králové	Czech_Republic	50.2	15.8	938	1.87	-0.25	0.99	1.02	-0.023
498	Kyiv-Goloseyev	Ukraine	50.4	30.5	1615	2.21	0.16	0.98	1	-0.025
68	Belsk	Poland	51.8	20.8	2638	2.36	0.08	0.97	0.96	-0.024
43	Lerwick	United_Kingdom	60.1	-1.2	2024	2.56	-1.16	0.97	0.99	-0.029
51	Reykjavík	Iceland	64.1	-21.9	1430	3.07	-1.31	0.93	0.91	-0.035
284	Vindeln	Sweden	64.2	19.8	727	2.18	-0.4	0.97	0.99	-0.036
105	Fairbanks	United_States	64.8	-147.9	546	2.52	-0.23	0.95	0.97	-0.037
199	Barrow	United_States	71.3	-156.6	189	2.36	-1.27	0.96	1	-0.033

3 Results and discussion

In this section, we evaluate the N20/OMPS total column ozone dataset generated using the NASA total ozone retrieval algorithm and the updated soft-calibration corrections described in Sect. 2.2.2. The primary objective is to assess whether the updated N20/OMPS retrievals provide a stable and consistent extension of the SNPP/OMPS-based NASA ozone record for 2018–2026. The evaluation is organized around five aspects.

First, N20/OMPS retrievals with and without the updated soft calibration are compared with SNPP/OMPS retrievals to demonstrate the impact of the calibration on total column ozone, scene reflectivity, and UVAI. This comparison reveals artifacts present in the uncorrected retrievals and the extent to which the updated soft calibration reduces these artifacts. Second, seasonal and monthly gridded comparisons with SNPP/OMPS are used to evaluate large-scale spatial consistency and possible geophysical dependencies. Third, long-term monthly time series and latitude-dependent difference fields are used to

https://doi.org/10.5194/essd-2026-802
Preprint. Discussion started: 18 November 2026
© Author(s) 2026. CC BY 4.0 License.


assess temporal stability and relative drift between N20/OMPS and SNPP/OMPS over the full study period. Fourth, the updated N20/OMPS retrievals are compared with the NOAA's N20/OMPS total ozone product to characterize product-level differences between the NASA and NOAA implementations. Finally, independent validation is performed using ground-based Dobson measurements.

The evaluation uses different matchup approaches depending on the comparison target, as described in Sect. 2.3. Satellite-to-satellite comparisons between N20/OMPS and SNPP/OMPS, as well as the product-level comparison between NASA N20 and NOAA N20, are performed using gridded fields. In contrast, the Dobson validation is performed using L2 swath retrievals matched directly to each station. For the gridded satellite analyses, daily, monthly, and seasonal fields are used for different purposes. Daily comparisons are used to examine spatial patterns, short-term anomalies, orbit-related features, and possible cross-track artifacts, while monthly and seasonal comparisons are used to quantify large-scale statistical consistency, geophysical dependence, and long-term stability. Retrievals are compared using collocated valid grid cells. The main statistical metrics include mean bias, standard deviation, root-mean-square error (RMSE), correlation coefficient, regression slope and intercept, and sample number. Additional diagnostics include row-wise differences, zonal mean differences, dependence on solar zenith angle, latitude, TCO amount, and season, as well as monthly difference time series and drift estimates. For Dobson validation, the same basic statistical quantities are calculated from the station-level satellite–ground matchups.

3.1 Impact of the updated soft calibration

The effect of the updated soft calibration is first evaluated by comparing N20/OMPS retrievals with and without the calibration against SNPP/OMPS (Fig. 1). The uncorrected N20/OMPS TCO field (Fig. 1b) reproduces the large-scale distribution observed by SNPP/OMPS (Fig. 1a) but has an approximately 2 % (6 DU) positive bias and distinct cross-track structures that produce discontinuities between orbits. The uncorrected N20/OMPS UVAI (Fig. 1e) also shows row-dependent structure and a systematic negative offset of about 0.6 relative to SNPP/OMPS (Fig. 1d). These features indicate residual wavelength- and row-dependent radiometric biases. After soft calibration, the N20/OMPS TCO field (Fig. 1c) is consistent with SNPP/OMPS

https://doi.org/10.5194/essd-2026-802
Preprint. Discussion started: 18 November 2026
© Author(s) 2026. CC BY 4.0 License.

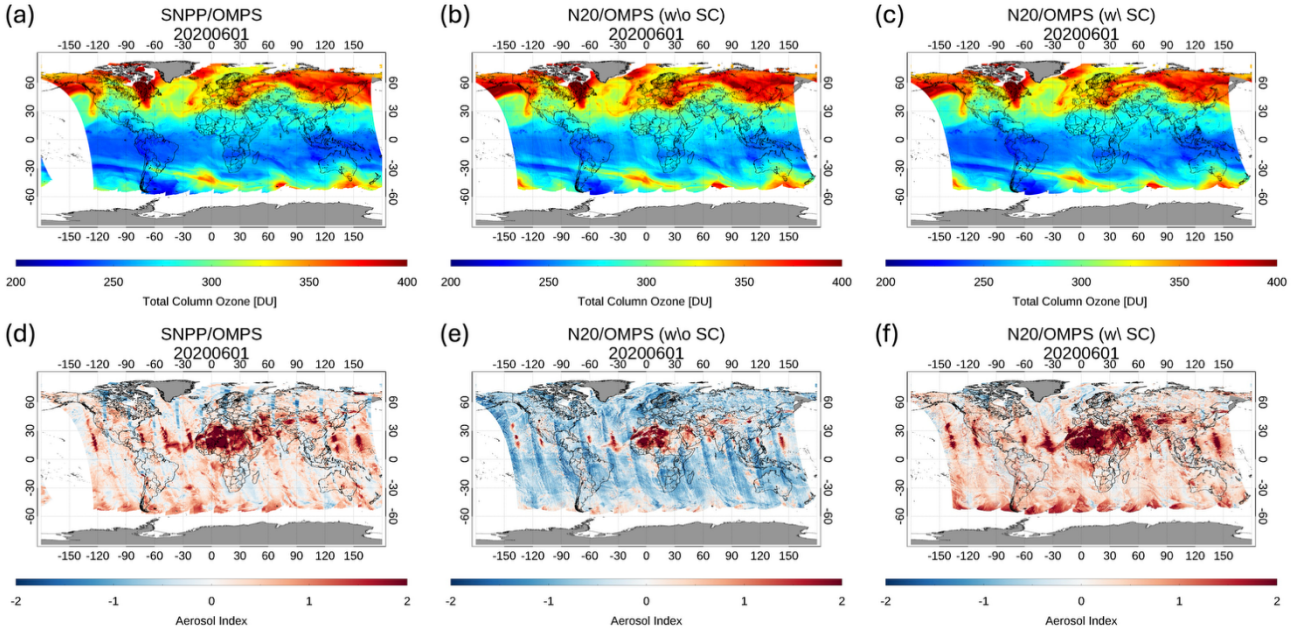


Figure 1. Daily distributions of total column ozone (TCO; upper panels) and ultraviolet aerosol index (UVAI; lower panels) on 1 June 2020 from SNPP/OMPS, N20/OMPS without soft calibration, and N20/OMPS with the updated soft calibration. The uncorrected N20/OMPS shows a positive TCO bias (~2 %) and discontinuity between orbits, along with a negative UVAI offset (~0.6) relative to SNPP/OMPS. The updated soft calibration improves agreement with SNPP/OMPS, reducing both the biases in TCO and UVAI while reducing orbit-to-orbit changes in TCO.

without evident additional cross-track artifacts, and the UVAI bias is substantially reduced (Fig. 1f). Thus, the calibration reduces radiometric biases and cross-track structure while preserving the large-scale ozone distribution.

Additional diagnostics were used to evaluate the row-dependent behavior of N20/OMPS after applying the soft-calibration adjustment (Fig. 2). This analysis used June 2019 data, which were not included in the soft-calibration adjustment derivation, and therefore provides an independent check of the calibration performance. To examine the general behavior of the retrievals under standard conditions, the analysis was restricted to retrievals with algorithm flag equal 1 in the tropical latitude range (|Latitude|<30°), but no additional cloud-fraction or aerosol filtering was applied. Because N20/OMPS and SNPP/OMPS have different cross-track sampling, the N20/OMPS 140 rows were grouped into 36 cross-track bins using consecutive row ranges, mostly four rows per bin, with narrower bins near nadir, to approximately match the SNPP/OMPS cross-track configuration before examining the row dependence. The row-dependent patterns of R331, UVAI, and TCO were then compared among SNPP/OMPS, N20/OMPS without the soft-calibration adjustment, and N20/OMPS with the soft-calibration adjustment. After applying the adjustment, the remaining N20–SNPP differences are small: TCO differs by about (+1.2) DU, and R331 differs by about (-0.005). The UVAI distribution shifts closer to the SNPP/OMPS values and becomes flatter across rows, consistent with the 360 nm adjustment derived from the UVAI probability distribution. These diagnostics confirm that the soft-calibration adjustment reduces row-dependent structures in reflectivity, UVAI, and TCO for data that were not used in deriving the

https://doi.org/10.5194/essd-2026-802
Preprint. Discussion started: 18 November 2026
© Author(s) 2026. CC BY 4.0 License.



adjustment. Hereafter, unless otherwise stated, all N20/OMPS results refer to retrievals processed with the final soft-calibration adjustment described in Sect. 2.2.2.

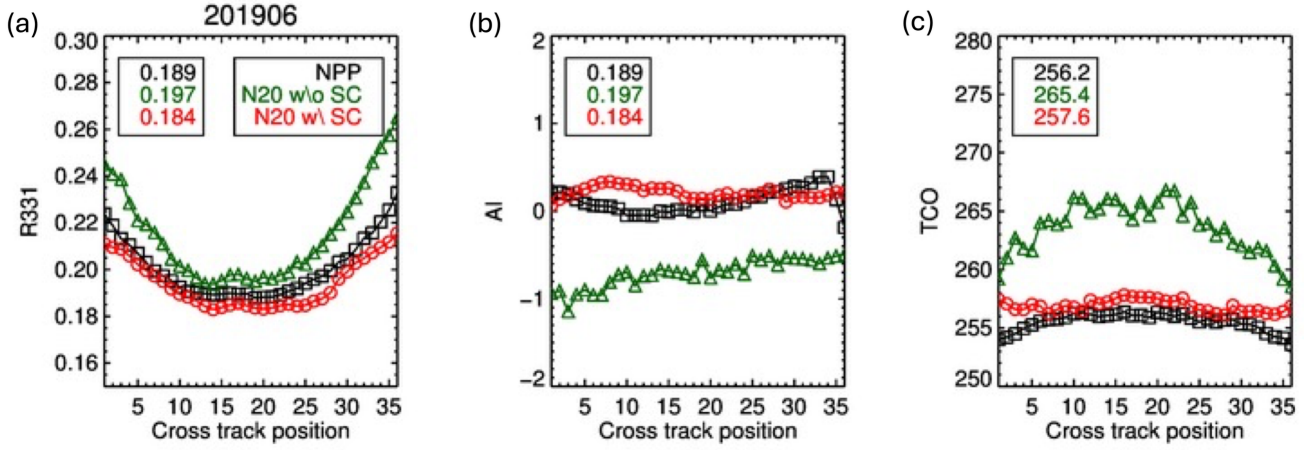


Figure 2. Row-dependent comparison of R331, UVAI, and TCO for SNPP/OMPS and N20/OMPS in June 2019. The June 2019 data were not used in deriving the soft-calibration adjustment. Retrievals are restricted to algorithm flag 1 and (|Latitude|<30), with no additional cloud-fraction or aerosol/UVAI filtering. The 140 N20/OMPS rows are rebinned into 36 row groups to approximately match the SNPP/OMPS cross-track configuration. Black, green, and red lines represent SNPP/OMPS, N20/OMPS without the soft-calibration adjustment, and N20/OMPS with the soft-calibration adjustment, respectively. The soft-calibration adjustment reduces row-dependent N20–SNPP differences in R331, UVAI, and TCO.

3.2 Spatial consistency with SNPP/OMPS

Monthly and seasonal gridded TCO fields were compared between N20/OMPS and SNPP/OMPS to evaluate whether the two sensors show consistent large-scale spatial patterns over the 2018–2025 period. The comparison uses the gridded products and standard retrieval filtering described in Sect. 2.3. No additional cloud-fraction or UVAI filtering was applied in this baseline spatial comparison, so the results represent the general product behavior. Seasonal mean fields were calculated for DJF, MAM, JJA, and SON to examine whether the N20–SNPP spatial differences vary systematically with season.

Figure 3 shows seasonal mean N20 minus SNPP total ozone difference maps together with the corresponding gridded scatterplots. The difference maps show no large-scale spatial artifacts or persistent latitude-dependent bias patterns. Most regions exhibit small N20–SNPP differences, indicating that the updated N20 retrievals provide seasonally consistent spatial agreement with the SNPP-based NASA ozone record. The seasonal gridded scatterplots further demonstrate strong agreement between the two sensors. For all seasons, the correlation coefficient is 1.00 and the regression relationship closely follows the one-to-one line. The RMSE ranges from approximately 0.69 to 0.73 DU, and the seasonal mean biases remain small, within about 0.3 %. The largest positive seasonal bias occurs in MAM, with a mean bias of about +0.26 %, whereas SON shows nearly zero mean bias. These results indicate that the N20/OMPS retrievals reproduce the seasonal spatial distribution of SNPP total ozone with high fidelity and without introducing notable seasonally dependent spatial artifacts.

https://doi.org/10.5194/essd-2026-802
Preprint. Discussion started: 18 November 2026
© Author(s) 2026. CC BY 4.0 License.

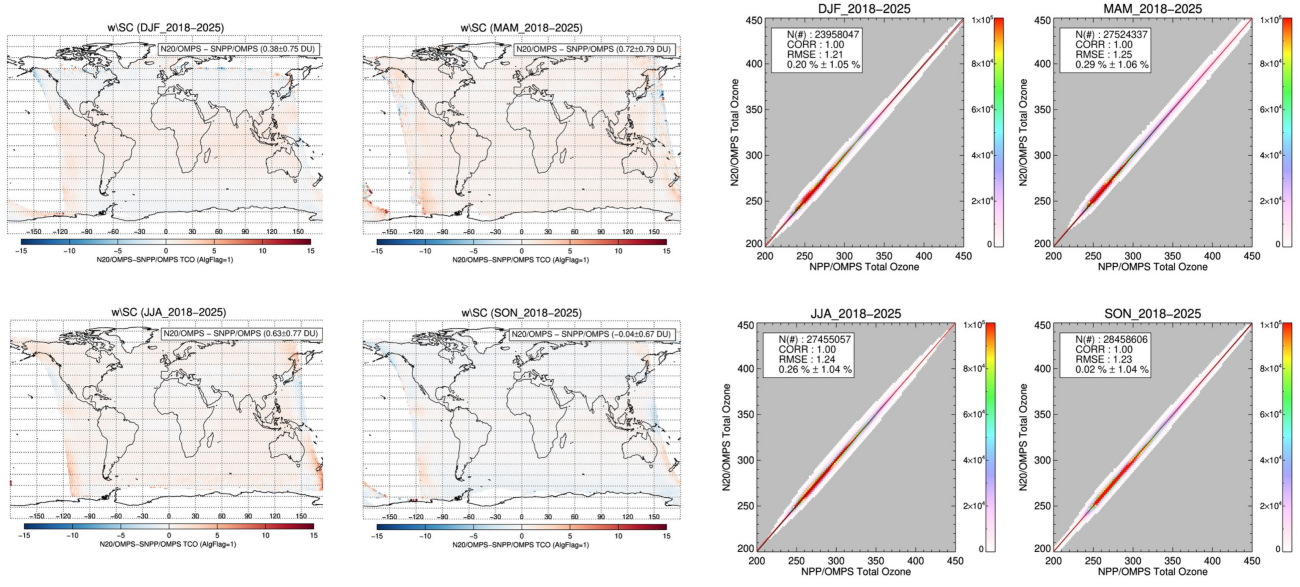


Figure 3. Seasonal comparison of N20/OMPS and SNPP/OMPS TCO for 2018–2025. Left panels show seasonal mean N20 minus SNPP TCO difference maps for DJF, MAM, JJA, and SON. The seasonal differences were calculated from the seasonal mean TCO fields of each sensor, which were generated by averaging monthly gridded fields derived from daily gridded retrievals. Right panels show scatterplots of collocated daily gridded N20/OMPS and SNPP/OMPS TCO values for all days within each season during 2018–2025. The comparisons use the standard gridded satellite-to-satellite matchup procedure described in Sect. 2.3.1. No additional cloud-fraction or UVAI filtering is applied. N20/OMPS shows strong agreement with SNPP/OMPS, with correlations of 1.00, RMSE values of about 0.7 DU, and seasonal mean biases within about 0.3 %.

3.3 Monthly statistics and geophysical dependence

To further check the consistency between the updated N20/OMPS and SNPP/OMPS retrievals, the statistical metrics described above were calculated from monthly gridded TCO fields for each calendar month using all available data from 2018 to 2025. Table 3 summarizes the number of collocated monthly grid cells, correlation coefficient, regression slope, RMSE, mean bias, and standard deviation of the N20 minus SNPP differences. The correlations are close to unity for all months, and the regression slopes range from 0.98 to 1.00, indicating that the updated N20 retrievals reproduce the dynamic range of SNPP total ozone throughout the year. The RMSE remains nearly constant, ranging from 1.19 to 1.26 DU, and the mean biases are small, ranging from −0.02 % to +0.36 %. The largest monthly mean bias occurs in March, while the biases are close to zero during September–November. These results are consistent with the seasonal comparisons in Sect. 3.2 and indicate good month-to-month agreement between N20/OMPS and SNPP/OMPS.

https://doi.org/10.5194/essd-2026-802
Preprint. Discussion started: 18 November 2026
© Author(s) 2026. CC BY 4.0 License.



Open Access Earth System Science Data Discussions

Table 3. Monthly comparison statistics for N20/OMPS and SNPP/OMPS TCO from 2018 to 2025. Statistics are calculated from monthly gridded fields generated from daily gridded retrievals with algorithm flag 1. No additional cloud-fraction or UVAI filtering is applied. Bias is defined as N20/OMPS minus SNPP/OMPS.

Months	*N*	*Correlation*	*Slope*	*RMSE [DU]*	*MBE [%]*	*BIAS [DU]*	*ERROR [DU]*	*EQU*
1	7810653	1	0.98	1.19	0.24	0.59	2.92	Y=0.98X + 5.6
2	7246649	1	0.99	1.21	0.3	0.76	3.01	Y=0.99X + 4.3
3	9313799	1	0.99	1.26	0.36	0.97	3.18	Y=0.99X + 2.9
4	9123115	1	0.99	1.25	0.28	0.77	3.11	Y=0.99X + 2.3
5	9087423	1	0.99	1.25	0.23	0.62	3.15	Y=0.99X + 2.2
6	8826417	1	0.99	1.24	0.27	0.76	3.13	Y=0.99X + 2.4
7	9060613	1	0.99	1.24	0.28	0.79	3.15	Y=0.99X + 2.7
8	9568027	1	1	1.22	0.23	0.66	3	Y=1.00X + 2.1
9	9961632	1	1	1.22	0.08	0.21	2.96	Y=1.00X + 1.4
10	9754877	1	0.99	1.23	0.01	-0.01	2.97	Y=0.99X + 1.6
11	8742097	1	0.99	1.24	-0.02	-0.1	3.08	Y=0.99X + 2.8
12	8900745	1	0.98	1.21	0.08	0.15	2.94	Y=0.98X + 4.8

We also examined whether the N20 minus SNPP total ozone difference depends on geophysical or observational conditions. The monthly gridded differences were analyzed as a function of solar zenith angle, SNPP total ozone, latitude, and calendar month for the February 2018–December 2025 period as shown in Fig. 4. For each bin, the mean N20 minus SNPP difference was calculated using all valid monthly grid cells. The results show no pronounced dependence on solar zenith angle, total ozone amount, or latitude. Across most bins, the mean differences remain generally within ±1 DU, indicating that N20/OMPS remains closely aligned with SNPP/OMPS across a broad range of observing and geophysical conditions.

A weak seasonal variation is observed, with smaller N20 minus SNPP differences during September–November, but its magnitude is small compared with the bin-to-bin variability and the overall spread of the differences. Overall, the monthly statistics and geophysical-dependence diagnostics show good consistency between N20/OMPS and SNPP/OMPS throughout the year.

https://doi.org/10.5194/essd-2026-802
Preprint. Discussion started: 18 November 2026
© Author(s) 2026. CC BY 4.0 License.

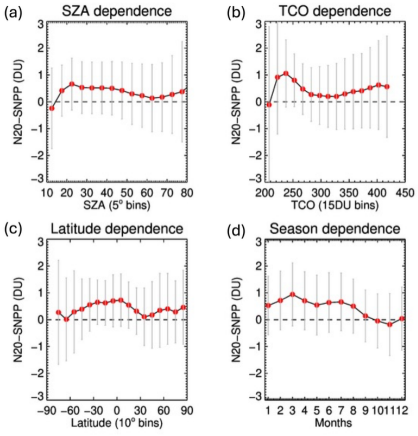


Figure 4. The differences between the monthly gridded TCO from N20/OMPS and that SNPP/OMPS as a function of (a) solar zenith angle, (b) SNPP TCO (c) latitude, and (d) calendar month during the period of February 2018–December 2025. For each bin, the mean difference is calculated using all valid monthly grid cells. Error bars indicate the spread of the differences within each bin.

3.4 Long-term stability of the N20/OMPS ozone record

The long-term stability of the N20/OMPS TCO was evaluated using monthly mean time series from 2018 to 2025. Figure 5 shows the monthly mean time series of N20 and SNPP TCO, deseasonalized TCO, and differences (N20 minus SNPP). N20/OMPS closely follows the seasonal cycle and interannual variability observed by SNPP/OMPS, with no apparent discontinuity associated with the aggregation change. The de-seasonalized time series also shows very similar temporal behavior between the two sensors, with trends of 0.304 DU yr^{-1} for N20/OMPS and 0.343 DU yr^{-1} for SNPP/OMPS. These similar de-seasonalized trends indicate that the N20 retrievals capture the same large-scale interannual ozone variability as SNPP. The monthly mean N20 minus SNPP difference is (0.41 ± 0.49) DU, indicating a small positive offset relative to SNPP. A linear fit to the monthly difference time series gives a relative drift of (-0.053) DU yr^{-1}, with a 95 % confidence interval of ([-0.096, -0.010]) DU yr^{-1}). Because the confidence interval does not include zero, this result indicates a small but statistically significant negative relative drift. However, the magnitude of the drift is small, corresponding to approximately (-0.18) % per decade relative to the mean total ozone column. Overall, these results indicate that N20/OMPS provide a consistent extension of the SNPP-based NASA TCO record, while the small residual relative drift should continue to be monitored in future long-term validation.

To evaluate whether the long-term agreement between N20/OMPS and SNPP/OMPS is consistent across latitude, monthly mean N20 minus SNPP differences were further examined in six 30° latitude bands as shown in Figure 6. The tropical and mid-latitude bands show relatively stable behavior, with mean offsets generally smaller than 1 DU and standard deviations of approximately 0.5 DU. The mean differences are (0.66 ± 0.53) DU for 30° S–0°, (0.53 ±0.48) DU for 0°–30° N, (0.43 ± 0.55) DU for 60° S–30° S, and (0.20 ± 0.57) DU for 30°–60° N. These results indicate that the small positive offset seen in the global mean comparison is broadly present across the tropics and mid-latitudes rather than being caused by compensating regional

https://doi.org/10.5194/essd-2026-802
Preprint. Discussion started: 18 November 2026
© Author(s) 2026. CC BY 4.0 License.



Open Access Earth System Science Data Discussions

biases. The fitted relative drifts are small in magnitude but generally negative. The 95 % confidence intervals indicate statistically significant negative drifts in several low- and mid-latitude bands, including 60° S–30° S, 30° S–0°, and 0°–30° N. However, the magnitudes remain small, ranging from approximately -0.05 to -0.08 DU yr^{-1}. Larger month-to-month variability is observed at high latitudes, especially in 90° S–60° S and 60° N–90° N, where the standard deviations are larger and the drift confidence intervals include zero. This larger high-latitude variability likely reflects increased retrieval sensitivity to high solar zenith angles, snow and ice scenes, polar ozone variability, and sampling differences between the two sensors. Overall, the latitude-band analysis supports the conclusion that N20/OMPS provide a stable extension of the SNPP-based TCO record across most latitude regions, with small residual negative drifts and larger uncertainty at high latitudes.

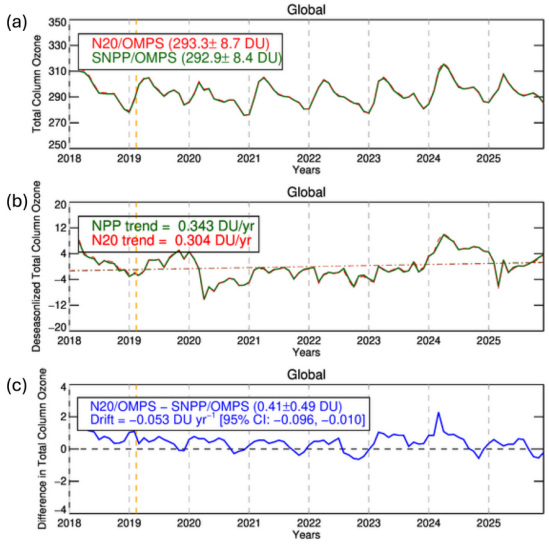


Figure 5. Global Monthly mean TCO time series for N20/OMPS and SNPP/OMPS from 2018 to 2025. The global mean is calculated using valid grid cells between 90° S and 90° N. The panels show monthly mean total column ozone, deseasonalized monthly mean TCO, and monthly mean N20 minus SNPP differences. The vertical dashed orange line marks the NOAA-20 OMPS-NM aggregation change from 104 to 140 cross-track macro-pixels in February 2019. The updated N20 retrievals closely follow the SNPP seasonal cycle and interannual variability, with a small mean offset and a small negative relative drift.

https://doi.org/10.5194/essd-2026-802
Preprint. Discussion started: 18 November 2026
© Author(s) 2026. CC BY 4.0 License.

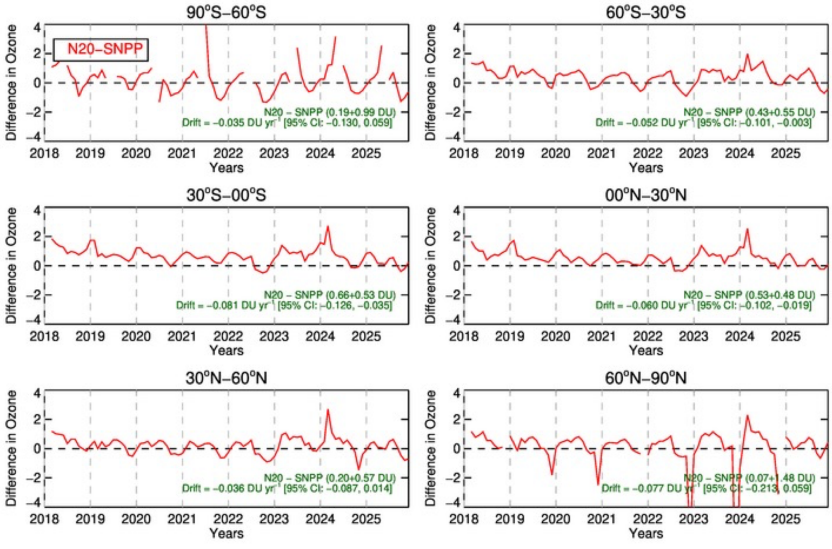


Figure 6. Monthly mean NOAA-20/OMPS minus SNPP/OMPS total column ozone differences in six 30° latitude bands from 2018 to 2025. Solid lines show the monthly mean differences, and dashed lines indicate the fitted linear trends for each latitude band. The tropical and mid-latitude bands exhibit small and stable positive offsets, generally below 1 DU, whereas the high-latitude bands show larger month-to-month variability. The fitted relative drifts are small in magnitude and generally negative in the low- and mid-latitude bands, while the high-latitude drift estimates are less robust because of larger variability.

Figure 7 further illustrates the temporal and latitudinal structure of the monthly mean N20 minus SNPP TCO differences using 1° latitude bins. Over most tropical and mid-latitude regions, the N20–SNPP differences remain small throughout the 2018–2025 period, generally within a few DU and without a persistent latitude-dependent discontinuity. Gray regions in the heatmap occur primarily at high latitudes and indicate latitude–time bins for which no valid paired N20–SNPP observations were available. The absence of a clear discontinuity around the February 2019 transition from the 104-row to 140-row NOAA-20 OMPS aggregation configuration suggests that this change did not introduce an obvious step change in the N20–SNPP TCO differences.

A noticeable positive N20–SNPP anomaly appears around March 2024 over a relatively broad latitude range. Daily latitude–time distributions for March and April 2024 was examined further in Appendix B and Fig. B1, confirming that the positive anomaly is concentrated mainly during approximately 18–28 March 2024 and is not present as a broad feature in April. The timing of the anomaly coincides with the NOAA-20 Rephasing Campaign, during which NOAA-20 temporarily did not meet its nominal orbit requirements (NASA Earthdata, 2024; NOAA OSPO, 2024). The timing and characteristics of the March 2024 anomaly are therefore consistent with a temporary data-quality degradation associated with the rephasing campaign rather than a persistent long-term drift in the N20/OMPS ozone record.

https://doi.org/10.5194/essd-2026-802
Preprint. Discussion started: 18 November 2026
© Author(s) 2026. CC BY 4.0 License.

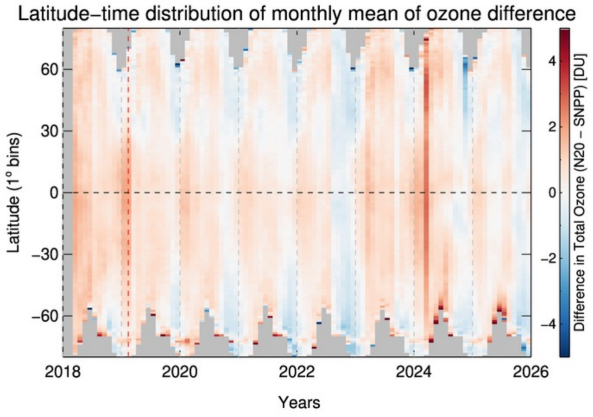


Figure 7. Latitude–time distribution of monthly mean N20/OMPS minus SNPP/OMPS TCO differences from 2018 to 2025. Differences are calculated in 1° latitude bins using retrievals with algorithm flag 1. Gray shading denotes latitude–month bins with no or insufficient retrievals after applying the algorithm flag 1 filter. The vertical dashed orange line marks the NOAA-20 OMPS-NM aggregation change from 104 to 140 cross-track macro-pixels in February 2019. The figure highlights the absence of a persistent latitude-dependent discontinuity and the temporally localized positive anomaly around March 2024.

3.5 Comparison with the NOAA N20 V8TOz total ozone product

As described in Sect. 2.3.2, the NOAA N20 V8TOz product was used for product-level comparison with our NASA N20 TCO. Zhang et al. (2023) derived soft-calibration corrections for the NOAA SNPP and NOAA N20 OMPS TCO using NASA SNPP as a reference. They reported good agreement between NASA SNPP and NOAA SNPP TCO, with a correlation coefficient of 0.998, a regression slope of 1.004, and a mean bias of (0.13 ± 1.67) DU. However, that comparison was based on only three days of data, and direct statistical comparisons of NOAA N20 total ozone against either NOAA SNPP or NASA SNPP were not explicitly provided. Therefore, in this study, NASA SNPP is used as a common reference to compare the consistency of NASA N20 and NOAA N20.

Figure 8 shows daily total ozone difference maps for NASA N20 minus NASA SNPP and NOAA N20 minus NASA SNPP on 12 September 2020. NASA N20 shows a near-zero mean difference relative to NASA SNPP, with a bias of (-0.01 ± 1.0) %, whereas NOAA N20 shows a larger positive bias of (+0.46 ± 1.8) %. The broader spread in the NOAA N20 comparison indicates larger differences relative to NASA SNPP for this case. Figure 9 extends this comparison to monthly aggregated daily gridded TCO fields for June 2020. Using NASA SNPP as the common reference, NOAA N20 shows good agreement, with a correlation coefficient of 0.98, an RMSE of 1.66 DU, and a mean bias of (+0.54) %. In comparison, NASA N20 shows stronger agreement with NASA SNPP, with a correlation coefficient of 1.00, an RMSE of 1.20 DU, and a mean bias of (+0.18) %. Thus, both the daily and monthly comparisons indicate that NASA N20 is more closely aligned with NASA SNPP than NOAA N20 for the cases examined here. This comparison should be interpreted with caution. The NASA N20 and NOAA N20 products differ not only in their soft-calibration tables, but also in Level-1B input data, calibration implementation, row configuration, native spatial resolution, and processing environment.

https://doi.org/10.5194/essd-2026-802
Preprint. Discussion started: 18 November 2026
© Author(s) 2026. CC BY 4.0 License.



Open Access Earth System Science Data Discussions

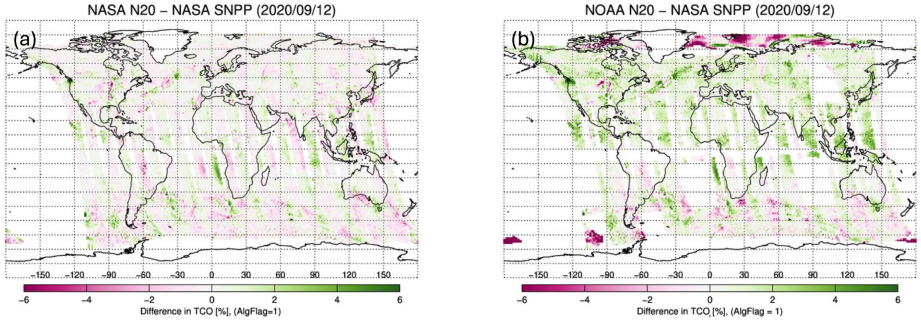


Figure 8. Daily TCO difference maps comparing NASA N20 and NOAA N20 against NASA SNPP as a common reference on 12 September 2020. The left panel shows NASA N20 minus NASA SNPP, and the right panel shows NOAA N20 minus NASA SNPP. NASA N20 shows a near-zero mean difference relative to NASA SNPP, whereas NOAA N20 shows a larger positive bias and broader spread for this case.

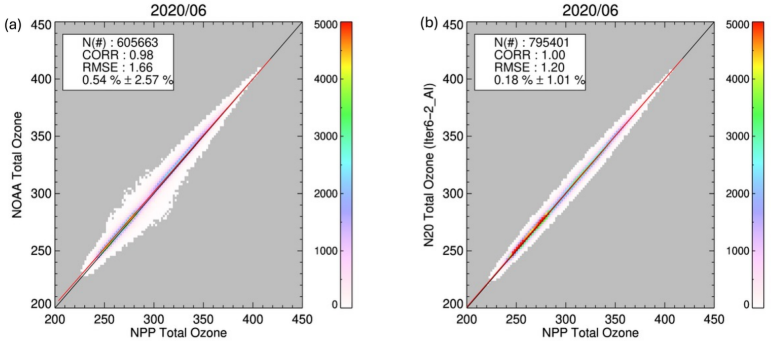


Figure 9. Monthly scatterplots for June 2020 using NASA SNPP as a common reference. Panel (a) compares NASA N20 with NASA SNPP, and panel (b) compares NOAA N20 with NASA SNPP. The scatterplots are based on collocated valid grid cells from daily gridded fields aggregated over the month. NASA N20 shows stronger agreement with NASA SNPP than NOAA N20 for this monthly comparison.

3.6 Validation against Dobson observations

The Dobson validation network and matchup procedure are described in Sect. 2.3.3. Briefly, 44 Dobson stations were retained after applying sampling and SNPP-based screening criteria for the independent validation of N20/OMPS dataset. Station-level comparison statistics for N20/OMPS, including RMSE, mean bias error, correlation coefficient, regression slope, relative bias, and drift, are summarized in Table 2.

The satellite–Dobson comparison was performed using the ensemble of 44 retained Dobson stations for the 2018–2025 period. Figure 10 shows scatterplot comparisons of daily mean TCO between the ground-based Dobson observations and the satellite retrievals. The left panel shows the comparison for N20/OMPS, and the right panel shows the comparison for SNPP/OMPS. The validation statistics are very similar for the two sensors. For N20/OMPS, the correlation coefficient is 0.96, the RMSE is 2.34 DU, and the mean relative bias is (0.18 ± 3.84) %. For SNPP/OMPS, the corresponding values are 0.96, 2.35 DU, and (-

https://doi.org/10.5194/essd-2026-802
Preprint. Discussion started: 18 November 2026
© Author(s) 2026. CC BY 4.0 License.



Open Access Earth System Science Data Discussions

0.03 ± 3.83) %. These results show that N20/OMPS has agreement with Dobson observations comparable to that of SNPP/OMPS when evaluated using the same ground-based reference network.

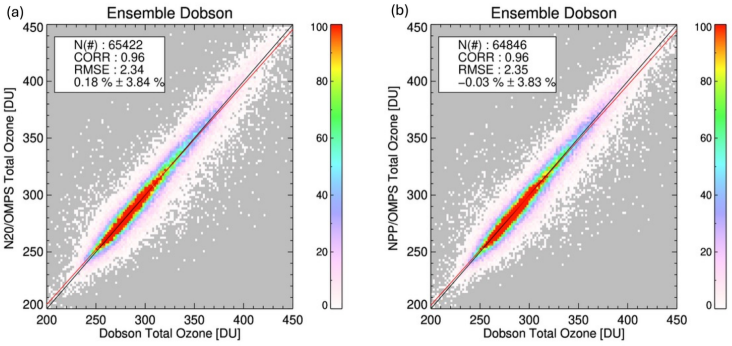


Figure 10. Comparison of N20/OMPS and SNPP/OMPS TCO retrievals with the ensemble of 44 retained Dobson stations for 2018–2025. The left panel shows the comparison between Dobson and N20/OMPS, and the right panel shows the comparison between Dobson and SNPP/OMPS. Both sensors show similar agreement with Dobson observations. The correlation coefficient, RMSE, and mean relative bias are 0.96, 2.34 DU, and (0.18 3.84) %, respectively, for N20/OMPS, and 0.96, 2.35 DU, and (-0.03 3.83) %, respectively, for SNPP/OMPS.

To examine whether N20/OMPS–Dobson differences depend on observational or geophysical conditions, the N20 minus Dobson and SNPP minus Dobson differences were analyzed as functions of cross-track row, solar zenith angle, total ozone, season, latitude, and cloud fraction (Fig. 11). The corresponding SNPP/OMPS–Dobson differences were analyzed in the same way and are shown as a reference benchmark, allowing us to determine whether the observed dependence patterns are specific to N20/OMPS or are common to both OMPS records. Because the N20/OMPS cross-track aggregation changed in February 2019, this dependence analysis was restricted to the period after the transition, from March 2019 to December 2025. In Figure 11, the red curves represent N20 minus Dobson differences, and the blue curves represent SNPP minus Dobson differences. Overall, the N20/OMPS–Dobson differences show no clear systematic dependence on cross-track row or season. The most evident dependences are observed for solar zenith angle, cloud fraction, and TCO amount. The N20/OMPS bias relative to Dobson becomes more negative as solar zenith angle increases. A similar increase in negative bias is observed with increasing cloud fraction, especially for cloud fraction greater than 0.8, where N20/OMPS underestimates Dobson TCO by up to about 4 %. This cloud-fraction dependence may be related to common retrieval sensitivity to cloud treatment, including the use of climatological cloud pressure under optically thick cloud conditions.

The dependence on TCO amount shows that the N20/OMPS–Dobson bias increases from about (-2) % to about (+1) % as TCO increases from approximately 225 to 400 DU. The lowest TCO bin, below 225 DU, shows a stronger negative bias, but this bin has relatively limited sampling compared with the other bins. Although it contains more than 50 matchups, it has fewer than 100 samples, whereas most other bins contain more than 2000 matchups. Therefore, the low-TCO result should be interpreted with caution because it may be affected by sampling uncertainty. A latitude dependence is also observed, with a

https://doi.org/10.5194/essd-2026-802
Preprint. Discussion started: 18 November 2026
© Author(s) 2026. CC BY 4.0 License.

positive bias at high southern latitudes and weak negative biases within about 2 % in the equatorial and northern latitude regions. The SNPP/OMPS–Dobson differences show broadly similar dependence patterns across these variables. This similarity indicates that the observed dependences are not specific to N20/OMPS and that N20/OMPS behaves consistently with the established SNPP/OMPS record in the Dobson comparison.

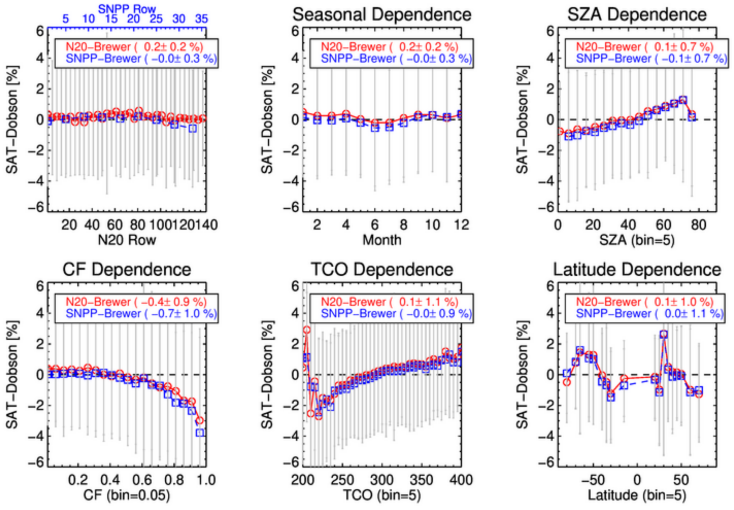


Figure 11. Dependence of N20/OMPS and SNPP/OMPS TCO differences relative to Dobson measurements on cross-track row, month, solar zenith angle (SZA), cloud fraction (CF), TCO amount, and latitude. Red circles denote N20/OMPS minus Dobson differences, and blue squares denote SNPP/OMPS minus Dobson differences. Gray vertical bars represent ±1 standard deviation within each bin. The two satellite records show broadly similar dependence patterns relative to Dobson, with larger or more variable differences under high-SZA, high-cloud-fraction, low-TCO, and high-latitude conditions.

The long-term temporal behavior of the satellite–Dobson differences was further examined using monthly mean time series. The upper panel of Figure 12 shows monthly mean TCO from N20/OMPS, SNPP/OMPS, and Dobson observations, and the lower panel shows the corresponding monthly mean satellite minus Dobson differences. Both N20/OMPS and SNPP/OMPS closely follow the Dobson seasonal cycle throughout the analysis period. The mean relative differences are (0.23 ± 0.55) % for N20 minus Dobson and (0.04 ± 0.50) % for SNPP minus Dobson. The estimated drifts are -0.10 % yr^{-1} for N20 minus Dobson and -0.07 % yr^{-1} for SNPP minus Dobson. These results indicate that the long-term biases relative to Dobson remain very small for both sensors. The slightly more negative drift for N20 is consistent with the small residual negative drift found in the N20 minus SNPP comparison, but the overall magnitude remains small. Most stations show drift values within about 0.1 % yr^{-1} except for several high-latitude stations in the Southern Hemisphere, where larger variability is observed. These high-latitude stations may contribute to the network-mean negative drift; therefore, the drift estimates should be interpreted with some caution and should continue to be monitored as the N20 record length increases.

https://doi.org/10.5194/essd-2026-802
Preprint. Discussion started: 18 November 2026
© Author(s) 2026. CC BY 4.0 License.



Open Access Earth System Science Data Discussions

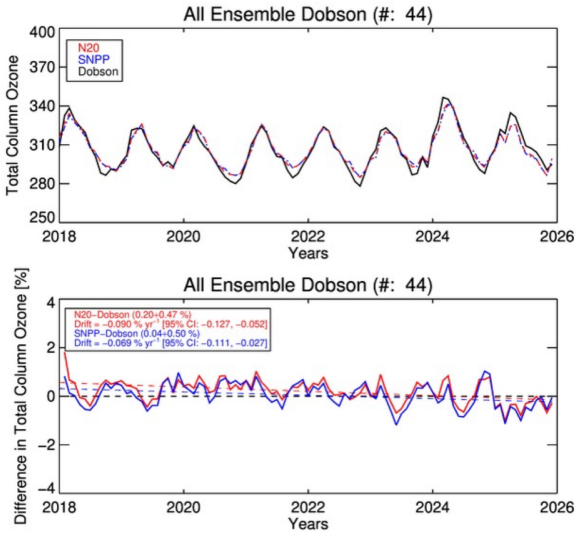


Figure 12. Long-term monthly mean comparison of N20/OMPS, SNPP/OMPS, and Dobson TCO for 2018–2025. The upper panel shows monthly mean TCO from N20/OMPS, SNPP/OMPS, and Dobson observations. The lower panel shows monthly mean satellite minus Dobson differences. Both OMPS records closely follow the Dobson seasonal cycle and show small mean relative differences, 0.23 ± 0.55 % for N20 minus Dobson and 0.04 ± 0.50 % for SNPP minus Dobson, with small negative drifts of −0.10 and −0.07 % yr⁻¹, respectively.

4 Conclusions

This study presents and evaluates a NOAA-20 OMPS-NM total column ozone dataset generated with the NASA total ozone retrieval algorithm and cross-calibrated against the SNPP/OMPS-NM. The primary goal is to assess whether N20/OMPS can provide a stable and consistent extension of the SNPP/OMPS-based NASA mapper TCO record during the JPSS era.

After application of the final soft-calibration adjustments, N20/OMPS shows close spatial and cross-track consistency with SNPP/OMPS in TCO, scene reflectivity, and UVAI.

Seasonal and monthly gridded comparisons demonstrate strong spatial and statistical consistency between N20/OMPS and SNPP/OMPS. N20/OMPS reproduces the seasonal spatial distribution of SNPP/OMPS TCO with correlations near unity, small RMSE values, and mean biases generally within a few tenths of a percent. The monthly statistics show good agreement throughout the year, and no pronounced dependence is found with respect to solar zenith angle, TCO amount, or latitude.

Long-term comparisons from 2018 to 2025 show that N20/OMPS closely follows the seasonal cycle and interannual variability observed by SNPP/OMPS. The global monthly mean N20 minus SNPP difference is 0.41 ± 0.49 DU. A linear fit to the monthly difference time series gives a small negative relative drift of −0.053 DU yr⁻¹ (95 % confidence interval: −0.096 to −0.010 DU yr⁻¹), corresponding to approximately −0.18 % per decade. Although statistically significant at the 95 % confidence level, the drift is small in magnitude. No clear discontinuity is observed across the February 2019 change from 104 to 140 cross-track

https://doi.org/10.5194/essd-2026-802
Preprint. Discussion started: 18 November 2026
© Author(s) 2026. CC BY 4.0 License.


macro-pixels. A positive anomaly in March 2024 is identified as a temporally localized feature likely associated with the NOAA-20 Rephasing Campaign rather than a persistent long-term drift.

The comparison with the NOAA N20 V8TOz product shows that both NASA N20 and NOAA N20 are broadly consistent with NASA SNPP, but NASA N20 is more closely aligned with NASA SNPP for the cases examined in this study. This result should be interpreted as a product-level comparison because the NASA and NOAA products differ in input L1B data, calibration tables, soft-calibration implementation, retrieval settings, row configuration, native spatial resolution, and processing environment.

Independent comparison with Dobson observations further supports the consistency of the N20/OMPS ozone record. Using an ensemble of 44 screened Dobson stations, N20/OMPS shows agreement with Dobson observations comparable to SNPP/OMPS, with a correlation coefficient of 0.96, an RMSE of 2.34 DU, and a mean relative bias of 0.18 ± 3.84 %. The corresponding SNPP/OMPS statistics are very similar, with a correlation coefficient of 0.96, an RMSE of 2.35 DU, and a mean relative bias of −0.03 ± 3.83 %. The dependence of the N20/OMPS–Dobson differences on cross-track row, solar zenith angle, TCO amount, season, latitude, and cloud fraction is broadly similar to that of SNPP/OMPS–Dobson, indicating that the observed dependence patterns are not specific to N20/OMPS.

Overall, these results demonstrate that the N20/OMPS TCO dataset provides a stable extension of the SNPP/OMPS-based NASA mapper TCO record, and the satellite and ground-based validation results confirm the effectiveness of the N20/OMPS calibration. The remaining small residual drift, high-latitude variability, and scene-dependent differences should continue to be monitored as the record length increases and as the same framework is extended to NOAA-21 and future JPSS OMPS instruments.

Appendix A Derivation of the N20/OMPS soft-calibration adjustments

This appendix provides the detailed scene-selection criteria, reference definitions, wavelength-specific equations, sign convention, and iterative procedure used to derive the N20/OMPS soft-calibration tables. For the 331 nm and ozone-sensitive wavelengths, the procedure has two stages: SNPP/OMPS nadir retrievals provide the external reference for correcting the N20/OMPS nadir measurements, after which the corrected N20 nadir retrievals provide the internal reference for deriving row-dependent adjustments across the N20 swath. The 360 nm adjustment is constrained independently by requiring the fitted N20 UVAI mean to approach zero. All corrections are derived and applied in N-value space; reflectivity (R), total column ozone (TCO), and UV aerosol index (UVAI) are used only as diagnostic constraints.

A1. Calibration samples and scene selection

The 104-row and 140-row N20 spatial aggregation configurations were calibrated separately because the aggregation scheme changed after orbit 6419 on 13 February 2019. The 104-row calibration was derived from June-September (JJAS) 2018 observations, and the 140-row calibration was derived from JJAS 2020 observations. To account for the different nadir

https://doi.org/10.5194/essd-2026-802
Preprint. Discussion started: 18 November 2026
© Author(s) 2026. CC BY 4.0 License.



Open Access Earth System Science Data Discussions

sampling of N20 and SNPP, N20 rows 50-55 in the 104-row configuration and rows 65-72 in the 140-row configuration were aggregated to approximate the SNPP nadir footprint defined by fields of view 17-19.

The analysis was restricted to low-aerosol, mostly clear, tropical dark-land scenes satisfying $30°\mathrm{S} < \text{latitude} < 30°\mathrm{N}$, solar zenith angle $< 50°$, terrain pressure > 900 hPa, $0 < R_{331} < 0.15$, and $|UVAI| < 1$. Snow-, ice-, water-, high-terrain-, and shadow-contaminated scenes were excluded. The UVAI is restricting its absolute magnitude reduces contamination from spectrally dependent aerosol and surface effects.

The complete screened sample was used to derive the adjustments at the ozone-sensitive wavelengths (312, 317, and 322 nm) and the UVAI-constrained adjustment at 360 nm. For the 331 nm adjustment, only the lowest 10% of the screened R_{331} distribution was retained to further reduce residual effects from clouds, aerosols, and surface heterogeneity.

A2. Adjustment definition and sign convention

For diagnostic quantity Q, define the pixel-level N20-minus-reference difference as

$$\Delta Q_{i,j} = Q_{i,j}^{\mathrm{N20}} - Q^{\mathrm{ref}},$$

where i indexes observations and j indexes cross-track rows. The reference is the matched SNPP nadir value in stage 1 or the corrected N20 nadir value in stage 2. For sample $\mathcal{S}_j$, the N-value correction is

$$\Delta N_{\lambda,j} = -\left\langle \left(\frac{\partial N_\lambda}{\partial Q}\right)_{i,j} \Delta Q_{i,j} \right\rangle_{i\in\mathcal{S}_j},$$

and it is applied as

$$N_{\lambda,i,j}^{\mathrm{corr}} = N_{\lambda,i,j}^{\mathrm{meas}} + \Delta N_{\lambda,j}.$$

The minus sign ensures that the applied correction opposes the diagnosed N20-minus-reference difference. Retrieved quantities are recalculated after applying the N-value correction; they are not corrected directly after retrieval.

A3. Reflectivity- and UVAI-constrained wavelengths

Let $\mathcal{S}_{10\%}^{\mathrm{N20,nad}}$ denote the lowest-10% N20 nadir sample, and let $\overline{R}_{331,10\%}^{\mathrm{SNPP,nad}}$ denote the mean R_{331} of the corresponding lowest-10% SNPP nadir sample. Because the reflectivity sensitivity is evaluated for each N20 observation before averaging, the stage-1 correction is

$$\Delta N_{331}^{\mathrm{nad}} = -\left\langle \left(\frac{\partial N_{331}}{\partial R_{331}}\right)_{i}^{\mathrm{N20,nad}} \left(R_{331,i}^{\mathrm{N20,nad}} - \overline{R}_{331,10\%}^{\mathrm{SNPP,nad}}\right) \right\rangle_{i\in\mathcal{S}_{10\%}^{\mathrm{N20,nad}}}$$

After this correction is applied, $\overline{R}_{331,10\%}^{\mathrm{N20,corr,nad}}$ becomes the internal reference. For row j, let $\mathcal{S}_{j,10\%}^{\mathrm{N20}}$ denote its lowest-10% N20 sample. The stage-2 correction is

https://doi.org/10.5194/essd-2026-802
Preprint. Discussion started: 18 November 2026
© Author(s) 2026. CC BY 4.0 License.

$$\Delta N_{331,j} = -\left\langle \left(\frac{\partial N_{331}}{\partial R_{331}}\right)_{i,j}^{\mathrm{N20}} \left(R_{331,i,j}^{\mathrm{N20}} - \overline{R}_{331,10\%}^{\mathrm{N20,corr,nad}}\right)\right\rangle_{i\in\mathcal{S}_{j,10\%}^{\mathrm{N20}}}.$$

The 360 nm adjustment is determined independently from N20 UVAI probability distributions over the complete screened sample. A Gaussian function is fitted to the N20 UVAI distribution for the nadir region and for each cross-track row j:

$$P_j(\mathrm{UVAI}) = A_j \exp\left[-\frac{(\mathrm{UVAI}-\mu_j)^2}{2\sigma_j^2}\right].$$

For the N20 nadir region and each cross-track row, $\Delta N_{360,j}$ is selected so that $\mu_j(\Delta N_{360,j}) \to 0$. Thus, the 360 nm correction does not use SNPP UVAI or corrected N20 nadir UVAI as a reference.

A4. Ozone-sensitive wavelengths

Below approximately 330 nm, radiance sensitivity to ozone increases rapidly. For the non-reference channels, wavelength-specific TCO is obtained from the retrieval residuals:

$$X_{312} = X_{317} + \frac{\mathrm{res}_{312}}{S_{312}}, \qquad X_{322} = X_{317} + \frac{\mathrm{res}_{322}}{S_{322}},$$

where X is TCO, res_λ is the wavelength-specific N-value residual, and $S_\lambda = \partial N_\lambda / \partial X$ is the ozone sensitivity. Differences in ozone-profile sensitivity among these wavelengths are neglected in this empirical adjustment.

For $\lambda \in \{312,317,322\}$ nm, the matched SNPP nadir TCO retrieved at 317 nm, $\overline{X}_{317}^{\mathrm{SNPP,nad}}$, is the stage-1 reference. Because sensitivity and ozone difference are evaluated for each N20 observation before averaging,

$$\Delta N_\lambda^{\mathrm{nad}} = -\left\langle S_{\lambda,i}^{\mathrm{N20,nad}} \left(X_{\lambda,i}^{\mathrm{N20,nad}} - \overline{X}_{317}^{\mathrm{SNPP,nad}}\right)\right\rangle_{i\in\mathcal{S}^{\mathrm{N20,nad}}}.$$

After these corrections are applied, the corrected N20 nadir 317 nm TCO, $\overline{X}_{317}^{\mathrm{N20,corr,nad}}$, becomes the stage-2 internal reference. The row-dependent correction is

$$\Delta N_{\lambda,j} = -\left\langle S_{\lambda,i,j}^{\mathrm{N20}} \left(X_{\lambda,i,j}^{\mathrm{N20}} - \overline{X}_{317}^{\mathrm{N20,corr,nad}}\right)\right\rangle_{i\in\mathcal{S}_j^{\mathrm{N20}}}.$$

The adjustments are derived independently at 312, 317, and 322 nm using the complete screened sample. This procedure reduces wavelength-dependent ozone differences and artificial cross-track structure without directly modifying retrieved TCO.

A5. Iteration and final calibration tables

The wavelength- and row-dependent corrections are derived iteratively. At each iteration, the accumulated N-value corrections are applied in the N20 retrieval; reflectivity, wavelength-specific TCO, and UVAI are recalculated; remaining differences from the applicable SNPP or corrected-N20-nadir reference are evaluated at 331, 312, 317, and 322 nm; the remaining fitted N20 UVAI offset from zero is evaluated at 360 nm; and incremental corrections are added to the calibration table. The 331 nm

https://doi.org/10.5194/essd-2026-802
Preprint. Discussion started: 18 November 2026
© Author(s) 2026. CC BY 4.0 License.



reflectivity correction is established first, after which the ozone-sensitive and UVAI-constrained corrections are refined using the updated retrieval diagnostics.

If $\Delta N_{\lambda,j}^{(k)}$ is the incremental correction at iteration k, the accumulated correction after K iterations is

$$C_{\lambda,j}^{(K)} = \sum_{k=1}^{K} \Delta N_{\lambda,j}^{(k)}.$$

Iterations continue until the incremental corrections are small and the residual row-dependent structures in R_{331}, TCO, and UVAI are sufficiently reduced. Convergence is typically achieved within five to six iterations. The final accumulated corrections define separate wavelength- and row-dependent soft-calibration tables for the 104-row and 140-row N20 configurations.

Appendix B March 2024 NOAA-20 rephasing anomaly

A noticeable positive N20–SNPP anomaly appears around March 2024 over a relatively broad latitude range. To further diagnose the March 2024 feature, daily latitude–time distributions of N20 minus SNPP total ozone differences were examined for March and April 2024 (Fig. B1). In March, the positive difference becomes apparent in mid-March and is most pronounced during approximately 18–28 March, extending over a broad range of latitudes and locally exceeding 5 DU. In contrast, the corresponding April analysis does not show a similarly broad positive anomaly, indicating that the March feature was temporally localized rather than persistent. The timing of this anomaly coincides with the NOAA-20 Rephasing Campaign. According to official data alerts, NOAA-20 executed a propulsive maneuver on 20 March 2024 to begin a rephasing campaign intended to provide approximately 180° separation between NOAA-20 and NOAA-21. During this campaign, NOAA-20 drifted at a lower altitude for approximately 16 days, and an orbit-raising maneuver was planned for 4 April 2024 to return the spacecraft to the correct altitude. NOAA also noted that NOAA-20 would not meet its orbit requirements during the rephasing period and that users should exercise caution when using NOAA-20 science data. The timing and characteristics of the March 2024 N20–SNPP anomaly are therefore consistent with a temporally localized data-quality degradation associated with this rephasing campaign, rather than a persistent long-term drift in the updated N20/OMPS ozone record.

https://doi.org/10.5194/essd-2026-802
Preprint. Discussion started: 18 November 2026
© Author(s) 2026. CC BY 4.0 License.

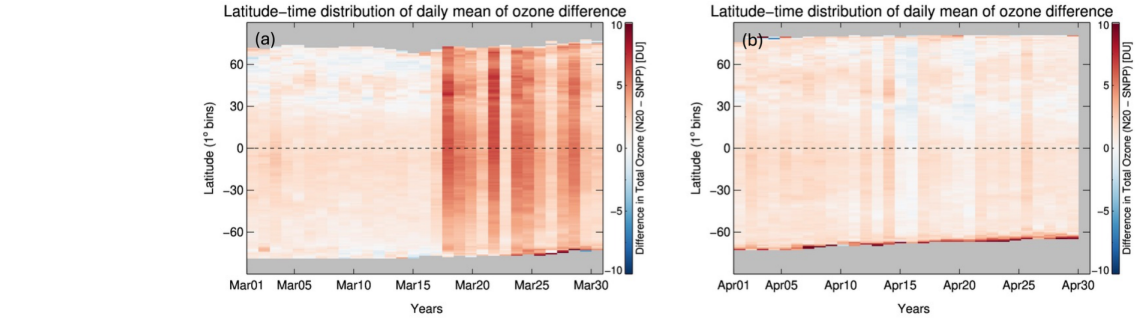


Figure B1. Daily latitude–time distributions of N20/OMPS minus SNPP/OMPS TCO differences for March and April 2024. Differences are calculated in 1° latitude bins using retrievals with algorithm flag 1, and the same color scale is used for both months. In March 2024, a broad positive N20–SNPP anomaly appears mainly during approximately 18–28 March and locally exceeds 5 DU. In contrast, the corresponding April 2024 analysis does not show a similarly broad positive anomaly

Data availability

The NOAA-20 OMPS-NM total column ozone dataset generated with the NASA total ozone retrieval algorithm and updated soft-calibration corrections is available from the NASA Goddard Earth Sciences Data and Information Services Center (GES DISC) at https://doi.org/10.5067/T4BRYY6L5HFD (Baek and Li, 2026; last access: 2 October 2026).

Detailed descriptions of the file structure, dimensions, variable definitions, quality-flag bit assignments, and data-access options are provided in the NOAA-N20 OMPS NMTO3-L2 product README (NASA GES DISC, 2026).

The corresponding SNPP/OMPS total column ozone product used as the NASA reference dataset is available from NASA GES DISC at https://doi.org/10.5067/0WF4HAAZ0VHK (McPeters, 2017; last access: 2 October 2026).

Ground-based total ozone observations used for validation are available from the World Ozone and Ultraviolet Radiation Data Centre (WOUDC) at https://doi.org/10.14287/10000004 (WMO/GAW Ozone Monitoring Community, 2026; last access: 8 October 2026).

The NOAA OMPS Version 8 Total Ozone Environmental Data Record is available from the NOAA Comprehensive Large Array-data Stewardship System (CLASS) under the JPSS_OZONE data family at https://www.class.noaa.gov/saa/products/search?datatype_family=JPSS_OZONE (NOAA CLASS, 2026; last access: 2 October 2026).

https://doi.org/10.5194/essd-2026-802
Preprint. Discussion started: 18 November 2026
© Author(s) 2026. CC BY 4.0 License.



Author contribution

KB designed and implemented the N20/OMPS retrieval and soft-calibration procedure, performed the retrieval tests and validation analyses, and prepared the manuscript. CL conceived and supervised the study and contributed to the design of the retrieval and calibration approach. NAK contributed to the calibration strategy, product evaluation, operational implementation, and public release of the dataset. GL provided guidance on the total ozone retrieval algorithm and the interpretation of the retrieval results. GJ provided expertise on OMPS instrument calibration and Level-1B data. BLF contributed to the evaluation and quality assessment of the retrieved data. JRZ and SMF contributed to the evaluation and interpretation of the long-term ozone record and trend results. All authors reviewed and commented on the manuscript

Competing interests

The authors declare that they have no conflict of interest.

Acknowledgements

This research has been partially supported by NASA's “Long Term Measurement of Ozone” project.

References

Baek, K. and Li, C.: OMPS-N20 L2 NM Ozone (O3) Total Column swath orbital V2, NASA Goddard Earth Sciences Data and Information Services Center (GES DISC) [data set], https://doi.org/10.5067/T4BRYY6L5HFD, 2026.

Bhartia, P. K. and Wellemeyer, C. W.: OMI Algorithm Theoretical Basis Document, Volume II, Chapter 2, NASA Goddard Space Flight Center, Greenbelt, Maryland, USA, https://doi.org/10.5067/AURA/OMI/DOC/ATBD-OMI-02, 2002.

Bojkov, R. D., Mateer, C. L., and Hanson, A.: Comparison of ground-based and Total Ozone Mapping Spectrometer measurements used in assessing the performance of the global ozone observing system, J. Geophys. Res.-Atmos., 93, 9525–9533, https://doi.org/10.1029/JD093iD08p09525, 1988.

Bovensmann, H., Burrows, J. P., Buchwitz, M., Frerick, J., Noël, S., Rozanov, V. V., Chance, K. V., and Goede, A. P. H.: SCIAMACHY: Mission objectives and measurement modes, J. Atmos. Sci., 56, 127–150, https://doi.org/10.1175/1520-0469(1999)056<0127:SMOAMM>2.0.CO;2, 1999.

Brion, J., Chakir, A., Daumont, D., Malicet, J., and Parisse, C.: High-resolution laboratory absorption cross section of O3: Temperature effect, Chem. Phys. Lett., 213, 610–612, https://doi.org/10.1016/0009-2614(93)89169-I, 1993.

Burrows, J. P., Weber, M., Buchwitz, M., Rozanov, V., Ladstätter-Weißenmayer, A., Richter, A., DeBeek, R., Hoogen, R., Bramstedt, K., Eichmann, K.-U., Eisinger, M., and Perner, D.: The Global Ozone Monitoring Experiment (GOME): Mission concept and first scientific results, J. Atmos. Sci., 56, 151–175, https://doi.org/10.1175/1520-0469(1999)056<0151:TGOMEG>2.0.CO;2, 1999.

https://doi.org/10.5194/essd-2026-802
Preprint. Discussion started: 18 November 2026
© Author(s) 2026. CC BY 4.0 License.



685 Crutzen, P. J.: The role of NO and NO2 in the chemistry of the troposphere and stratosphere, Annu. Rev. Earth Pl. Sc., 7, 443–472, https://doi.org/10.1146/annurev.ea.07.050179.002303, 1979.

Daumont, D., Brion, J., Charbonnier, J., and Malicet, J.: Ozone UV spectroscopy I: Absorption cross-sections at room temperature, J. Atmos. Chem., 15, 145–155, https://doi.org/10.1007/BF00053756, 1992.

Fang, X., Pyle, J. A., Chipperfield, M. P., Daniel, J. S., Park, S., and Prinn, R. G.: Challenges for the recovery of the ozone
690 layer, Nat. Geosci., 12, 592–596, https://doi.org/10.1038/s41561-019-0422-7, 2019.

Fioletov, V. E., Kerr, J. B., Hare, E. W., Labow, G. J., and McPeters, R. D.: An assessment of the world ground-based total ozone network performance from the comparison with satellite data, J. Geophys. Res.-Atmos., 104, 1737–1747, https://doi.org/10.1029/1998JD100046, 1999.

Fioletov, V. E., Labow, G., Evans, R., Hare, E. W., Köhler, U., McElroy, C. T., Miyagawa, K., Redondas, A., Savastiouk, V.,
695 Shalamyansky, A. M., Staehelin, J., Vanicek, K., and Weber, M.: Performance of the ground-based total ozone network assessed using satellite data, J. Geophys. Res.-Atmos., 113, D14313, https://doi.org/10.1029/2008JD009809, 2008.

Flynn, L., Long, C., Wu, X., Evans, R., Beck, C. T., Petropavlovskikh, I., McConville, G., Yu, W., Zhang, Z., and Niu, J.: Performance of the Ozone Mapping and Profiler Suite (OMPS) products, J. Geophys. Res.-Atmos., 119, 6181–6195, https://doi.org/10.1002/2013JD020467, 2014.

700 Frith, S. M., Kramarova, N. A., Stolarski, R. S., McPeters, R. D., Bhartia, P. K., and Labow, G. J.: Recent changes in total column ozone based on the SBUV Version 8.6 Merged Ozone Data Set, J. Geophys. Res.-Atmos., 119, 9735–9751, https://doi.org/10.1002/2014JD021889, 2014.

Jacob, D. J., Logan, J. A., and Murti, P. P.: Effect of rising Asian emissions on surface ozone in the United States, Geophys. Res. Lett., 26, 2175–2178, https://doi.org/10.1029/1999GL900450, 1999.

705 Kramarova, N. A., Nash, E. R., Newman, P. A., Bhartia, P. K., McPeters, R. D., Rault, D. F., Seftor, C. J., Xu, P. Q., and Labow, G. J.: Measuring the Antarctic ozone hole with the new Ozone Mapping and Profiler Suite (OMPS), Atmos. Chem. Phys., 14, 2353–2361, https://doi.org/10.5194/acp-14-2353-2014, 2014.

Levelt, P. F., van den Oord, G. H. J., Dobber, M. R., Mälkki, A., Visser, H., de Vries, J., Stammes, P., Lundell, J. O. V., and Saari, H.: The Ozone Monitoring Instrument, IEEE T. Geosci. Remote, 44, 1093–1101,
710 https://doi.org/10.1109/TGRS.2006.872333, 2006.

Malicet, J., Daumont, D., Charbonnier, J., Parisse, C., Chakir, A., and Brion, J.: Ozone UV spectroscopy II: Absorption cross-sections and temperature dependence, J. Atmos. Chem., 21, 263–273, https://doi.org/10.1007/BF00696758, 1995.

McPeters, R. D., Bhartia, P. K., Krueger, A. J., Herman, J. R., Schlesinger, B. M., Wellemeyer, C. G., Seftor, C. J., Jaross, G., Taylor, S. L., Swissler, T., Torres, O., Labow, G., Byerly, W., and Cebula, R. P.: Nimbus-7 Total Ozone Mapping Spectrometer
715 (TOMS) Data Products User's Guide, NASA Reference Publication 1384, NASA, Washington, DC, USA, available at: https://ntrs.nasa.gov/citations/19960022782 (last access: 8 October 2026), 1996.

McPeters, R. D., Bhartia, P. K., Krueger, A. J., Herman, J. R., Wellemeyer, C. G., Seftor, C. J., Byerly, W., and Celarier, E. A.: Total Ozone Mapping Spectrometer (TOMS) Level-3 Data Products User's Guide, NASA/TP-2000-209896, NASA

https://doi.org/10.5194/essd-2026-802
Preprint. Discussion started: 18 November 2026
© Author(s) 2026. CC BY 4.0 License.

Goddard Space Flight Center, Greenbelt, Maryland, USA, available at: https://ntrs.nasa.gov/citations/20010044085 (last access: 2 October 2026), 2000.

McPeters, R. D., Bhartia, P. K., Haffner, D., Labow, G. J., and Flynn, L. E.: The Version 8.6 SBUV ozone data record: An overview, J. Geophys. Res.-Atmos., 118, 8032–8039, https://doi.org/10.1002/jgrd.50597, 2013.

McPeters, R. D.: OMPS-NPP L2 NM Ozone (O3) Total Column swath orbital V2, NASA Goddard Earth Sciences Data and Information Services Center (GES DISC) [data set], https://doi.org/10.5067/0WF4HAAZ0VHK, 2017.

McPeters, R., Frith, S., Kramarova, N., Ziemke, J., and Labow, G.: Trend quality ozone from NPP OMPS: the version 2 processing, Atmos. Meas. Tech., 12, 977–985, https://doi.org/10.5194/amt-12-977-2019, 2019.

NASA Earthdata: NOAA-20 Rephasing Campaign Scheduled March 20 to April 4, 2024, Data Alert, available at: https://www.earthdata.nasa.gov/data/alerts-outages/noaa-20-rephasing-campaign-scheduled-march-20-april-4-2024 (last access: 2 October 2026), 2024.

NASA GES DISC: README Document for Suomi-NPP OMPS NMTO3-L2 Product, Version 2.1, last revised 6 July 2017, NASA Goddard Earth Sciences Data and Information Services Center, available at: https://snpp-omps.gesdisc.eosdis.nasa.gov/data/SNPP_OMPS_Level2/OMPS_NPP_NMTO3_L2.2/doc/README.OMPS_NPP_NMTO3_L2.2.pdf (last access: 2 October 2026), 2017.

NASA GES DISC: README Document for NOAA-N20 OMPS NMTO3-L2 Product, Version 2.0, last revised 26 June 2026, NASA Goddard Earth Sciences Data and Information Services Center, available at: https://omps.gesdisc.eosdis.nasa.gov/data/NOAA20_OMPS_Level2/OMPS_N20_NMTO3_L2.2/doc/README.OMPS_N20_NMTO3_L2.2.pdf (last access: 12 November 2026), 2026.

NOAA CLASS: Joint Polar-Orbiting Satellite System (JPSS) data products: OMPS Total Column EDR (V8TOZ-EDR), JPSS_OZONE data family, NOAA Comprehensive Large Array-data Stewardship System [data set], available at: https://www.class.noaa.gov/release/data_available/jpss/index.htm (last access: 8 October 2026), 2026.

NOAA Office of Satellite and Product Operations (OSPO): NOAA-20 Rephasing Maneuver Burn Planned for March 19th and 20th 2024, ESPC Notification, issued 13 March 2024, available at: https://www.ospo.noaa.gov/data/messages/2024/03/MSG_20240313_2116.html (last access: 8 October 2026), 2024.

Seftor, C. J., Jaross, G., Kowitt, M., Haken, M., Li, J., and Flynn, L. E.: Postlaunch performance of the Suomi National Polar-orbiting Partnership Ozone Mapping and Profiler Suite (OMPS) nadir sensors, J. Geophys. Res.-Atmos., 119, 4413–4428, https://doi.org/10.1002/2013JD020472, 2014.

Vasilkov, A., Joiner, J., Spurr, R., Bhartia, P. K., Levelt, P., and Stephens, G.: Evaluation of the OMI cloud pressures derived from rotational Raman scattering by comparisons with other satellite data and radiative transfer simulations, J. Geophys. Res.-Atmos., 113, D15S19, https://doi.org/10.1029/2007JD008689, 2008.

Veefkind, J. P., Aben, I., McMullan, K., Förster, H., de Vries, J., Otter, G., Claas, J., Eskes, H. J., de Haan, J. F., Kleipool, Q., van Weele, M., Hasekamp, O., Hoogeveen, R., Landgraf, J., Snel, R., Tol, P., Ingmann, P., Voors, R., Kruizinga, B., Vink, R., Visser, H., and Levelt, P. F.: TROPOMI on the ESA Sentinel-5 Precursor: A GMES mission for global observations of the

© Author(s) 2026. CC BY 4.0 License.



atmospheric composition for climate, air quality and ozone layer applications, Remote Sens. Environ., 120, 70–83, https://doi.org/10.1016/j.rse.2011.09.027, 2012.

World Meteorological Organization (WMO): Scientific Assessment of Ozone Depletion: 2014, Global Ozone Research and Monitoring Project–Report No. 55, 416 pp., Geneva, Switzerland, available at: https://csl.noaa.gov/assessments/ozone/2014/report/index.html (last access: 8 October 2026), 2014.

WMO/GAW Ozone Monitoring Community: World Meteorological Organization–Global Atmosphere Watch Programme (WMO-GAW)/World Ozone and Ultraviolet Radiation Data Centre (WOUDC), Total Ozone – Daily Observations [data set], https://doi.org/10.14287/10000004 (last access: 8 October 2026), 2026.

Xiong, X., Beck, T., and Pan, C.: Status of NOAA-20 Ozone Mapping and Profiler Suite (OMPS) sensor data calibration and evaluation, Proc. SPIE, 11127, 111271B, https://doi.org/10.1117/12.2529386, 2019.

Zhang, Z., Niu, J., Flynn, L. E., Beach, E., and Beck, T.: An approach to track instrument calibration and produce consistent products with the version-8 total column ozone algorithm (V8TOZ), Atmos. Meas. Tech., 16, 2919–2941, https://doi.org/10.5194/amt-16-2919-2023, 2023.